Mineralium Deposita

Reactive transport model of the formation of oxide type Ni-laterite profiles (Punta Gorda, Moa Bay, Cuba)

--Manuscript Draft--

Manuscript Number:	MIDE-D-16-00020R4
Full Title:	Reactive transport model of the formation of oxide type Ni-laterite profiles (Punta Gorda, Moa Bay, Cuba)
Article Type:	Regular Articles
Corresponding Author:	Cristina Domènech Universitat de Barcelona SPAIN
Corresponding Author Secondary Information:	
Corresponding Author's Institution:	Universitat de Barcelona
Corresponding Author's Secondary Institution:	
First Author:	Cristina Domènech
First Author Secondary Information:	
Order of Authors:	Cristina Domènech
	Salvador Galí
	Cristina Villanova-de-Benavent
	Josep Maria Soler
	Joaquín Antonio Proenza
Order of Authors Secondary Information:	
Funding Information:	
Abstract:	Oxide type Ni-laterite deposits are characterized by a dominant limonite zone with goethite as the economically most important Ni ore mineral, and a thin zone of hydrous Mg silicate-rich saprolite beneath the magnesium discontinuity. Fe, less soluble, is mainly retained forming goethite, while Ni is redeposited at greater depth in a Fe(III) and Ni rich serpentine (serpentine II) or in goethite, where it adsorbs or substitutes for Fe in the mineral structure. Here, a 1D reactive transport model, using Crunchflow, of Punta Gorda oxide type Ni-laterite deposit (Moa Bay, Cuba) formation is presented. The model reproduces the formation of the different laterite horizons in the profile from an initial, partially serpentinized peridotite, in 106 years, validating the conceptual model of the formation of this kind of deposits in which a narrow saprolite horizon rich in Ni-bearing serpentine is formed above peridotite parent rock and a thick limonite horizon is formed over saprolite. Results also confirm that sorption of Ni onto goethite can explain the weight percent of Ni found in the Moa goethite. Sensitivity analyses accounting for the effect of key parameters (composition, dissolution rate, carbonate concentration, quartz precipitation) on the model results are also presented. It is found that aqueous carbonate concentration and quartz precipitation significantly affects the laterization process rate, while the effect of the composition of secondary serpentine or of mineral dissolution rates is minor. The results of this reactive transport modeling have proven useful to validate the conceptual models derived from field observations.
Response to Reviewers:	Please see attachment.

Powered by Editorial Manager® and ProduXion Manager® from Aries Systems Corporation

Manuscript With Track Changes

Click here to download Manuscript With Track Changes
manuscript_4threvision_trackchanges.docx

Reactive transport model of the formation of oxide type Ni-laterite profiles (Punta Gorda, Moa Bay, Cuba)

Cristina Domènech[1], Salvador Galí[1], Cristina Villanova-de-Benavent[1], Josep M. Soler[2,3], Joaquín A. Proenza[1]

[1]Departament de Mineralogia, Petrologia i Geologia Aplicada, Facultat de Ciències de la Terra, Universitat de Barcelona (UB), C/ Martí i Franquès s/n - 08028 Barcelona, Catalonia, Spain

[2]Institute of Environmental Assessment and Water Research, IDAEA, CSIC, Jordi Girona 18-26, 08034, Barcelona, Catalonia, Spain

[3]Associated Unit: Hydrogeology Group (UPC-CSIC)

CORRESPONDING AUTHOR

Cristina Domènech – cristina.domenech@ub.edu. Telf +34 934 021 341. Fax + 34 934 021 340

ABSTRACT

Oxide type Ni-laterite deposits are characterized by a dominant limonite zone with goethite as the economically most important Ni ore mineral, and a thin zone of hydrous Mg ~~silicate~~ silicate-rich saprolite beneath the magnesium discontinuity. Fe, less soluble, is mainly retained forming goethite, while Ni is redeposited at greater depth in a Fe(III) and Ni rich serpentine (serpentine II) or in goethite, where it adsorbs or substitutes for Fe in the mineral structure. ~~Nevertheless, these mechanisms are still not clear. In this paper~~Here, a 1D reactive transport model, using ~~-~~Crunchflow, of Punta Gorda oxide type Ni -laterite deposit (Moa Bay ~~mining area~~, Cuba) formation is presented. ~~Simulations are done with Crunchflow.~~ The model reproduces the formation of the different laterite horizons ~~observed~~ in the profile from an initial, partially serpentinized peridotite, in 10^6 years, validating the conceptual model of the formation of this kind of deposits in which a narrow saprolite horizon rich in Ni-bearing serpentine is formed above peridotite parent rock and a thick limonite horizon is formed over saprolite. Results also confirm that sorption of Ni onto goethite ~~surface~~ can explain the ~~percentages~~ weight percent of Ni found in the Moa goethite. ~~of Moa.~~

Sensitivity ~~cases~~ analyses accounting for the effect of ~~some~~ key parameters (composition, dissolution rate, carbonate concentration, quartz precipitation) on the model results are also presented. It is ~~observed~~ found that aqueous carbonate concentration and quartz precipitation significantly affects the laterization process

rate, while the effect of the composition of secondary serpentine ~~II composition~~ or of mineral dissolution ~~mineral~~ rates is minor.

~~Although still preliminary,~~ The results of this reactive transport modeling have ~~been~~ proven~~d~~ ~~to be~~ useful to validate the conceptual models derived from field observations.

KEYWORDS,

Oxide type Ni-laterites, Reactive Transport Modeling, Sorption, Goethite, Cuba

~~ACKNOWLEDGEMENTS~~

~~This research has been financially supported by FEDER Funds, the Spanish projects CGL2009-10924 and CGL2012-36263 and Catalan project 2014-SGR-1661. We are grateful to Prof. J.P. Golightly, M.Cathelineau and an anonymous reviewer for their careful reviews and constructive criticism of the original manuscript.~~

~~1.~~ Introduction

Nickel laterite deposits are an important source of nickel and cobalt (Golightly 1981, 2010; Freyssinet et al. 2005, Lambiv Dzemua et al. 2013) and have potential ~~are considered worthy targets~~ for Sc and platinum group element by-products ~~exploration~~ (Aiglsperger et al. 2016~~ and references therein~~).

Ni-laterite deposits formed from the chemical and mechanical weathering of ultramafic rocks exposed to the surface under favorable topography and climatic ~~and topographic~~ conditions. Laterite formation is controlled by ~~different factors, namely~~ intrinsic or extrinsic factors (Freyssinet et al. 2005, Moore et al. 2012, Butt and Cluzel 2013). Intrinsic factors include, among others, the chemical and mineralogical composition of protolith (mainly peridotite~~s~~), the dissolution rate~~s~~ of ~~their forming~~ minerals and the~~ir~~ surface area. The geological context where laterite~~s~~ develop, the hydrological properties of the terrain (controlling ~~the~~ water flow), the climate (temperature and rainfall) and the duration of the weathering process are examples of extrinsic factors that may condition ~~the~~ laterite formation.

According to Golightly (1981, 2010) a typical Ni-laterite profile consists, from bottom to top of: a) partially or totally serpentinized ultramafic rock (protolith) characterized by unweathered minerals; b) saprolite horizon ~~formed by a regolith material~~ with textural features inherited from the protolith and dominated by secondary Si- and Mg- ~~bearing~~ minerals; and c) limonitic horizon composed mainly ~~by~~ of goethite that evolves to hematite with time. The interaction of slightly acidic meteoric water~~s (slightly acidic)~~ with the ultramafic bed-rock~~s~~ cause~~s~~ the release of Mg, Si and Ni, which are transported downwards. In particular, Ni, less soluble, is redeposited at depth producing ~~different~~ Ni-~~-~~enriched zones. In the saprolite zone, Ni is mainly found in garnierite and/or secondary Ni-rich lizardite (serpentine II) and Ni-smectite~~s~~ (Pelletier 1996, Wells et al. 2009, Villanova-de-Benavent et al. 2014)~~, and references therein)~~. In the limonitic horizon, Ni is mainly retained by goethite, either adsorbed or substituting Fe in the mineral structure, and by minor Mn- oxyhydroxides (Roqué-Rosell et al. 2010; Dublet et al. 2015). ~~and references therein).~~

Ni-laterites are usually classified according to their dominant Ni-bearing mineralogy in a) hydrous silicate type, b) clay type and c) oxide type (Brand et al. 1998; Freyssinet et al. 2005). Oxide type deposits, ~~objective of~~discussed in this contribution, are characterized by a dominant limonite horizon with goethite as the economically most important Ni ore mineral. These deposits represent about 60% of the current total Ni laterite resources, with mean grades ranging from 1.0 to 1.6 wt% Ni (Butt and Cluzel 2013)~~ and references therein)~~.

Ni-laterites ~~have been~~ formed, or are currently forming (Butt and Cluzel 2013~~)~~), under humid tropical climate~~s~~, where rainfall is higher than 1000 mm/y and temperature~~s~~ ranges between 15-31 ºC (Freyssinet et al. 2005; Thorne et al. 2012).

The mechanisms controlling the retention of Ni in goethite determine the mobility of the metal and the supergene enrichment of the Ni-bearing phases in the laterite horizons (Roqué-Rosell et al. 2010; Dublet et al. 2012). However, the~~se~~ mechanisms ~~are still not clear~~controlling Ni mobility remain partly understood.

The Ni-goethite association has been explained either by sorption of Ni onto the goethite surface (Cornell 1991; Rose and Bianchi-Mosquera 1993; Bryce et al. 1994; Coughlin and Stone 1995; Beukes et al. 2000; Trivedi and Axe 2001; Trivedi et al. 2001; Buerge-Weirich et al. 2002; Fisher et al. 2007; Arai 2008; Marcussen et al. 2009) or by the incorporation of Ni into the goethite structure or ~~by~~ both (Manceau et al. 2000; Singh et al. 2002; Carvalho-e-Silva et al. 2002, 2003; Fan and Gerson 2011; Dublet et al. 2012). Sorption of Ni on goethite has been studied both in natural and synthetic goethite by means of sorption experiments and spectroscopic techniques. Ni sorbs onto goethite forming inner~~-~~-sphere mononuclear bidentate complexes (Trivedi et al. 2001; Xu et al. 2007), and sorption increases from pH 5 to 8 (Rose and Bianchi-Mosquera 1993; Beukes et al. 2000; Buerge-Weirich et al. 2002; Arai 2008). Sorption of Ni onto goethite has been modelled by considering Langmuir isotherms (Trivedi et al. 2001), a Diffuse Layer Model (Bryce et al. 1994; Buerge-Weirich et al. 2002; Marcussen et al. 2009; Rajapaksha et al. 2012) or a Triple Layer Model (Coughlin and Stone 1995).

The incorporation of Ni in the goethite structure ~~could be~~ is facilitated by the similar ionic radii between Fe^{3+} (0.64Å) and Ni^{2+} (0.69Å). However, even this small difference ~~induces~~ changes ~~in~~ cell parameters, and together with the difference in charge between both cations, limits the maximum amount of Ni in goethite (Dublet et al. 2015). According to Cornell (1991), 15% of sites occupied by Fe in goethite can be substituted by other cations without destabilizing the goethite structure. Manceau et al. (2000) studied ~~a~~ natural goethite by extended X-~~ray~~ Ray A~~a~~bsorption F~~f~~ine S~~s~~tructure (EXAFS) and showed ~~observed~~ that Ni was partially incorporated in the goethite structure ~~of goethite~~. Singh et al. (2002) demonstrated ~~an~~ up to 5 mol % isomorphic substitution of Ni^{2+} in the FeOOH structure ~~up to 5 mol %,~~ which was limited by ~~the~~ changes in the next-nearest-neighbour coordination environment. Differential thermal (DTA), thermal gravimetric (~~DTA~~TGA ~~TGA~~) and EXAFS analyses of ~~a~~ natural lateritic goethite ~~of lateritic origin~~ (1.8-4.1 mol% Ni) ~~performed~~ by Carvalho-e-Silva et al. (2002, 2003) suggested that the charge imbalance

could be compensated by the incorporation of H^+ into the goethite structure. Fan and Gerson (2011) indicated that ~~the~~ Ni associated with goethite in Philippine laterite~~s~~ was substituting Fe within its structure. Dublet et al. (2012) and Cathelineau et al. (2016) studied the speciation of Ni ~~along the~~in a New Caledonian laterite profile and observed Ni-goethite as the predominant Ni-bearer.

Bryce et al. (1994) considered that although sorption ~~processes~~ should be reversible, ~~due to~~because of aging or hysteresis Ni might not be completely released from goethite surface~~s~~. Dublet et al. (2015) stated that the incorporation of Ni in goethite may be affected by the sequence of dissolution-precipitation reactions forming goethite. Therefore, ~~and despite the~~in spite of evidence~~s~~ of both sorption of Ni on the goethite surface and its incorporation in the structure, there is still a lack of understanding of these processes. ~~that might occur simultaneously.~~

In order ~~to corroborate or discard hypotheses and~~ to test the validity of conceptual models derived from field and/or experimental observations, reactive transport ~~modeling~~ and geochemical modeling ~~codes have been~~has proven~~d~~ ~~as~~ successful ~~tools~~ (Soler and Lasaga 1998; Corbella et al. 2004). There are several computer codes available to perform reactive transport or geochemical calculations (Steefel et al. 2015), although none of them can ~~cope~~ consider ~~with~~ all hydro-geochemical processes ~~occurring~~ simultaneously. ~~In recent years, some studies focused on modeling of weathering processes.~~ Soler and Lasaga (1996, 1998) developed one dimensional models of bauxite (Al-laterite) formation, describing the alteration of a granitic protolith and the formation of the bauxite and saprolite horizons over long time scales (10^6 years) using mineral reaction kinetics ~~from the literature~~. Fletcher et al. (2006) performed a simple two-mineral model to study how ~~spheroidal~~ weathering can transform intact bedrock into saprolite. The model coupled physical processes (e.g. fracturing) to chemical processes (e.g. mineral dissolution) and the rate of displacement of the reaction front ~~resulted~~ was shown to depend on the composition of the reactant fluid where ~~(being~~ O_2 and CO_2 are the most critical components in the ~~studied~~ case of a Puerto Rico quartz diorite regolith~~)~~. ~~Later on,~~ Lebedeva et al. (2007) incorporated saprolite-forming reactions and developed a four-mineral model to predict rates of formation of saprolite, ~~and~~ whereas Fletcher and Brantley (2010) developed a simplified one dimensional model to study ~~the~~ a weathering profile, including vertical fluid transport, kinetic reaction~~s~~ and erosion.

Navarre-Sitchler et al. (2011) used the reactive coupled transport ~~model~~ code CrunchFlow to simulate the chemical and physical transformations ~~occurring~~ during ~~the~~ weathering of a basaltic rock and compared their results with field observations of alluvial terraces ~~of~~ in Costa Rica, where erosion was not

significant. They used a 1D model of a total length of 100 mm and observed that for porosities higher than 9%, mineral reaction kinetics dominated over transport, and that the advance of the weathering front ~~rate~~ was controlled by the rate at which porosity was created.

Moore et al. (2012) modeled the dissolution of minerals in a granitic soil and in a granitic saprolite with the reactive transport model FLOTRAN. The modeled reaction front depth was highly dependent on the precipitation rate of secondary minerals and on ~~the~~ fluid flow. Moreover, they had to use reduced reaction rates, compared with rates from laboratory studies, ~~reduce the laboratory rates by decreasing the surface reactive areas~~ to fit the field observations. They concluded that reactive transport models can be used to understand the long-lived (10^6 years) mineral weathering processes given that they consider the simultaneous non-linear processes. ~~can cope with simultaneous processes that do not behave linearly.~~

In this study, a reactive transport model is used to simulate the formation of the oxide type Punta Gorda Ni-laterite deposit ~~of Punta Gorda~~ from an initial partially serpentinized peridotite at constant temperature (25ºC). The Punta Gorda deposit is part of the Moa Bay mining area, one of the largest reserves of nickel and cobalt in the world (Linchenat and Shirakova 1964; Lavaut 1998; Lewis et al. 2006; Proenza et al. 2007; Aiglsperger et al. 2016), and probably the best known example of Ni-laterite deposits of oxide type ~~in commercial production~~ (Gleeson et al. 2003).

The main objective of this contribution is to test a conceptual model for the formation of ~~this kind of~~oxide type Ni-laterite deposits and to identify and quantify, the key parameters affecting the development of the different laterite horizons. Moreover, ~~and~~ by considering that Ni is sorbed onto goethite, we aim ~~at checking~~to determine whether this process could account for the amount of Ni found in the goethite at Punta Gorda.

In this paper, we present a ~~first~~ modeling exercise that provides ~~new~~ valuable insights into the understanding of the formation of Ni-laterite deposits. The~~is~~ modeling ~~exercise~~ consists of a set of one dimensional models in which rain water infiltrates and flows vertically downwards simulating the infiltration through fractures and cracks. Formation of the goethite and saprolite horizons is achieved by ~~the~~ dissolution of primary minerals and ~~the~~ precipitation of secondary minerals. No solid solutions have been included for ~~a sake of~~ simplicity. Porosity changes reflecting different molar volumes of dissolving/precipitating minerals are taken into account.

Due to fact that the model is ~~only~~ one dimensionale~~d~~, it ~~the model~~ does not account for the formation of typical saprolite corestones as lateral water flow and matrix diffusion processes are not considered. Water

is allowed to equilibrate with ~~atmospheric~~ air along the whole domain, simulating unsaturated conditions. Calculations have been carried out for a ~~total~~ time span of 10^6 years. Past climatic changes, ~~(~~such as variations in precipitation regime~~)~~, ~~erosion~~ erosion, or collapse due to ~~a severe~~ increase in porosity in ~~of~~ the upper part of laterite profile are not considered.

The 1D models described here~~conforming this modeling exercise~~ differ in ~~the~~ values for ~~assigned to~~ several parameters that ~~in~~ preliminary work had ~~been~~ identified as having a significant~~-~~ role in the formation of laterite profiles, such as ~~(~~solubility constants, dissolution rates, CO_2(g), precipitation of quartz.~~,..).~~ A~~One of these models (~~ Reference case~~)~~ model is explained in detail whereas ~~, while~~ the results of the other~~s~~ models ~~(Sensitivity cases)~~ are compared to the results of the Reference case.

~~This modeling exercise must be considered as a first step in the modeling of laterite profiles. The results will be of great utility when designing future models with higher complexity in terms of dimension (2D, 3D), number and type of processes (matrix diffusion, more complete mineralogies, Ni coprecipitation in goethite), formation of solid solutions or chemical components (Mn, Co, Al,…).~~

~~2.~~ The Punta Gorda Ni-laterite deposit

The Punta Gorda Ni-Co laterite deposit is located in the Moa Bay mining area (northeast of Cuba; ~~)~~ ~~(~~Fig.1). The Moa Bay laterite deposits are part of a larger province of nickel laterite~~s~~ in northeast Cuba. The deposits ~~were~~ developed over serpentinized harzburgite of Moa-Baracoa ophiolitic massif (Proenza et al. 1999; Marchesi et al. 2006) with weathering and laterization commencing during the Miocene (Lewis et al. 2006; Proenza et al. 2007) ~~and references therein)~~. The elevation ~~above sea level~~ of the peneplain surface of the deposits varies from 60 to 950 m above sea level, and the weathering mantle can reach a total thickness of more than 50 m in the laterite profile (Linchenat and Shirakova 1964; Golightly et al., 2008b~~-~~).

This deposit can be classified as oxide type (Oliveira et al. 2001; Rojas-Purón et al. 2012; Aiglsperger et al. 2016). ~~and~~ As with~~as~~ many northeastern Cuban deposits, the typical vertical section ~~of a profile~~ consists of four principal horizons, from bottom to top: (1) parent rock serpentinized peridotite, (2) saprolite, (3) lower and upper limonite and (4) ferricrete or duricrust (Lewis et al. 2006; Proenza et al. 2007; Aiglsperger et al. 2016; ~~) (~~Fig. 2a). Occasionally, within a ~~the~~ profile some gabbro bodies weather~~ed~~ to bauxite ~~appear~~. Ni and Co are mainly in the limonite zone but the siting of ~~doubts about the detailed distribution of~~ metals (adsorbed or in solid solution) ~~still~~ remains debated.

The Punta Gorda deposit has been extensively studied (Oliveira et al. 2001; Galí et al. 2007; Roqué-Rosell et al. 2010; Rojas-Purón et al. 2012; Aiglsperger et al. 2016). The m~~M~~ineralogy was characterized by qualitative and quantitative X-R~~r~~ay ~~powder~~ diffraction, optical and scanning electron microscopy (SEM~~-EDS~~) and electron ~~micro~~probe microanalysis (E~~M~~PMA; ~~) (~~Galí et al. 2007). Concentrations of ~~relevant~~ major and minor elements ~~(in wt.%)~~ as well as trace elements ~~(in ppm or ppb)~~ in parent rocks and weathering products of Ni~~-~~-laterite profiles were measured ~~analyzed~~ by Aiglsperger et al. (2016). ~~Analytical conditions for the SEM and EMPA are summarized in Roqué-Rosell et al. (2010) and Villanova-de-Benavent et al. (2014).~~

The ~~M~~mineralogical composition of the studied profile in Punta Gorda is shown in Fig. 2b~~. As seen, mineral composition changes from bottom to top~~. The ~~M~~main minerals of the parent ~~rock~~ serpentinized peridotite are forsterite, enstatite, serpentine and maghemite (Sample M10). The ~~S~~saprolite horizon is dominated by serpentine and goethite (Sample M9), whereas ~~and~~ in limonite and ferricrete horizons, goethite and hematite are the main minerals, although other minor phases such as pyrochroite, gibbsite, quartz, Mn-oxyhydroxide aggregate (lithiophorite, “lithiophorite–asbolane intermediates”) and asbolane (Roqué-Rosell et al. 2010) are also found (samples M8 to M1).

~~Olivine and enstatite represent~~ T~~t~~he parent rock from which the Ni-laterite profile in the Moa district originated consists of ~~. This is a~~ partially serpentinized ophiolitic harzburgite (70% $Mg_9Fe_{0.95}Ni_{0.05}Si_5O_{20}$, 16% $Mg_9FeSi_{10}O_{30}$) including plagioclase-rich bodies,~~impregnated by plagioclase,~~ which was exposed to the surface during the late Miocene (≈ 10^7 years; ~~) (~~Lewis et al. 2006).

Serpentine minerals are ~~present as~~ politype 1T and 2H1 lizardite. Lizardite 1T is the dominant politype ~~and~~ whereas lizardite 2H1 is less crystalline and presents many stacking faults in its structure. The cell volume is slightly ~~big~~larg~~g~~er than that corresponding to the ideal end member $Mg_3Si_2O_5(OH)_4$, due to substitution of ~~some~~ Mg by Fe and minor Ni and Mn, as confirmed by chemical analyses. Two different types of serpentine have been identified. Serpentine I ~~represents the serpentine~~ formed by ~~due to the~~ alteration of forsterite and enstatite during a~~the~~ hydrothermal stage, whereas ~~and~~ serpentine II ~~the serpentine~~ formed after weathering of serpentine I. Serpentine II can be formed as a thermodynamically stable secondary phase in meteoric conditions, as shown in Villanova-de-Benavent et al. (2016a).

Serpentine I composition, ~~has been~~ calculated from ~~results obtained by~~ EPM~~MP~~A data ~~and considered equal to~~is $Mg_{2.85}Fe_{0.14}Ni_{0.01}Si_2O_5(OH)_4$. In serpentine II, Mg in octahedral coordination ~~position~~ is partially substituted by Fe^{3+} and Ni^{2+}. Serpentine II structural formulae calculated from E~~M~~PMA are

shown in Online resource 1~~Table 1~~. ~~As can be seen, s~~Serpentine II contains more Ni than serpentine I. The~~se~~ Ni-bearing serpentine~~s~~ (Srp-II), in addition to "garnierite~~s~~", is~~are~~ the main Ni ore~~s~~ in saprolite horizon of Ni-laterite deposits (~~e.g.~~ Golightly and Arancibia 1979; Pelletier 1996; Villanova-de-Benavent et al. 2014, 2016b). In ~~and in t~~the case of Punta Gorda deposit, this second generation of serpentine~~s~~ is the major Ni-bearing silicate phase in the saprolite horizon. Nickel content in Ni-rich serpentine ranges from 1 to 7 wt.% NiO, in contrast with ~~primary~~ serpentine I, which has the same Ni content ~~is no more enriched in Ni~~ than the olivine (~ 0.4 wt.%).

Iron oxides are ~~present as~~ maghemite, goethite and hematite. The refined cell parameter of maghemite, very similar to the accepted value of 8.3505 Å, indicates a composition near the ideal Fe_2O_3 (Galí et al. 2007). In near surface conditions, maghemite can form by ~~from the~~ oxidation of magnetite (Gehring et al. 2009, Lilova et al. 2012) that in turn, results from the hydration of primary olivine and pyroxene. Under atmospheric conditions, maghemite is transformed into goethite. Hematite (Fe_2O_3) has almost an ideal composition and structure, although it has a ~~presents a rather~~ low crystallite size (30 to 40 nm; ~~) (~~Galí et al 2007). Goethite (FeOOH), the major phase containing most of the Ni in this profile (from 0.8 to 4 wt.% with an average value of 1.23 wt.%), coexists with maghemite and hematite in limonite samples and with lizardite in samples M8 and M9 (Galí et al. 2007). Crystallographic studies indicate that there is some substitution (2-17%) of Fe by Al as the cell volume is always smaller than the accepted value for goethite. ~~Recently, an additional characterization of this goethite based on t~~The analysies of different diffraction peaks of goethite using ~~through~~ the Scherrer's relation ~~(eq. 1)~~ (Klug and Alexander 1962; Langford 1978; De Keijser et al. 1982; Louër et al. 1983) ~~has been done.~~

$$D_{hkl} = \frac{\lambda}{FWMH_{hkl} \times \cos\theta} \quad (1)$$

~~The Scherrer's relation allows the obtention of the mean shape and dimensions of crystallites (D_{hkl}, in nm) from the length of the radiation used (λ, in nm), the width of the hkl diffraction peak ($FWMH_{hkl}$, in radian units) and the diffraction angle (θ).~~ and ~~Us~~using values for the 110, 020, 120 and 130 ~~selected~~ peaks in the space group P_{bnm} (a=4.605 Å, b=9.96 Å and c=3.02 Å; ~~) (~~Fig. 3), and a value of λ[Kα1,Cu] of 1.5406 Å, yields an ~~the most approximate surface to the~~ ideal mean ~~particle is an~~ elongated prism in the **c** direction, with 8.7 nm in the **a** direction and 18.1 nm in **b** direction**.** The length in **c** could not be determined, but ~~morphological~~ observations have shown that the ~~morphological~~ c/b aspect -ratio ~~c/b~~ is not less than 4.5 (Strauss et al. 1997). With these data, the calculated specific surface for goethite is 84.8 m^2/g. If, instead of adjusting a prismatic shape, an elliptical cylinder elongated in the **c** direction is fitted

~~to the obtained directional dimensions~~, a specific surface of 87.2 m^2/g is obtained, which is ~~very~~ similar to the previous value.

The specific surface obtained by the BET (Brunauer-Emmet-Teller) method (Brunauer et al. 1938) for the same material is 65.2 m^2/g. As expected, the BET value is lower than the value calculated through X-~~ray~~ Ray ~~powder~~ diffraction which reflects the dimension of the coherent diffracting domains, rather than the dimension of the material particle that consists of an ~~usually is formed by~~ aggregate ~~ion~~ of several ~~d~~domains.

~~3.~~ Materials and methods

The reactive transport model presented in this work is based on the direct formation conceptual model described in Butt and Cluzel (2013). According to this model, oxide type Ni-laterite deposits form as a result of ~~a~~ continuous weathering of ~~a~~ partially serpentinized peridotite under tropical climate. During weathering, the water table is high and fluctuating, and erosion rates are low. The system is ~~well drained and~~ fully saturated. Meteoric water, in equilibrium with atmospheric O_2 and CO_2, flows through the profile at a constant rate. Therefore, Ni is expected to be released from olivine or serpentine I and retained by the formation of a Fe(III)-rich serpentine II and by sorption onto goethite, while Mg and Si are expected to be leached out of the system (Ulrich et al. 2014, Villanova-de-Benavent et al. 2016a) because of serpentine and silicate dissolution. ~~This might~~Dissolution can cause an increase in porosity that may accelerate the ~~occurring~~ processes due to the ~~corresponding~~ decreased ~~in the~~ solid/water ratio.

According to ~~the conceptual model described in~~ Butt and Cluzel (2013), Ni may be ~~further~~ leached from goethite ~~and form~~to garnierite deeper in the profile, and goethite may transform to hematite, ~~in special~~particularly in the upper most limonite horizon. Neither the formation of garnierite, nor the formation of hematite, is considered in this ~~first~~ model. ~~presented here.~~

Temperature is considered constant ~~and equal to~~at 25 ºC. According to Thorne et al. (2012), ~~the formation of~~ Ni-laterite forms ~~s occurs~~ in tropical areas where monthly temperatures are in the range of 22-31 ºC in the summer and between 15-27 ºC in the winter.

The partially serpentinized unweathered peridotite is composed of Ni-bearing forsterite, enstatite and serpentine I. ~~as representative mineral phases of the unweathered peridotite.~~ In our~~this~~ model, ~~the inclusion of~~ maghemite is not considered ~~has been discarded~~ given its low stability. Its precursor, magnetite is ~~has been~~ considered instead (Gehring et al. 2009). Serpentine I and magnetite ~~are supposed~~

~~to~~ formed during a previous hydrothermal serpentinization event~~period~~ (pre-weathering), ~~whose formation~~that is outside ~~of~~ the scope of this study.

~~3.1~~ Chemistry solver, modeled domain and hydrodynamic system

The ~~code~~ computer code used for the simulations is Crunchflow, a software package for simulating reactive transport ~~modeling~~ developed by Steefel and co-workers (Stefeel and Lasaga 1994; Stefeel 2009). This code can take into account ~~handle~~ aqueous speciation, surface complexation, ion exchange, mineral dissolution/precipitation and transport processes under fully saturated flow conditions and ~~different temperatures~~variable temperature (Steefel et al. 2015). A~~In the code, a~~ll mineral transformations are ~~always~~ treated as dissolution and precipitation reactions. Kinetic reaction rates, depending on reactive surface area, are used to describe these reactions. Transformations in the solid state (without dissolution/precipitation) are not considered. However, if reaction rates are fast compared to solute transport by ~~(~~advection, dispersion or~~,~~ diffusion~~)~~, when the dissolution of a mineral can cause~~s~~ supersaturation of the solution with respect to another phase,~~,~~ this new phase will precipitate at the same location as that of the dissolving mineral, causing an effect similar to a potential solid-state transformation. The code uses an integrated finite difference discretization to solve the advection-dispersion-reaction differential equations that link flow, solute transport and geochemical processes. Total porosity (ϕ_T) is ~~may be~~ updated after each time step according to eq. ~~2~~1, where N_m is the number of minerals in the model (Navarre-Sitchler et al. 2011) and ϕ_m, the volume fractions of minerals.

$$\phi_T = 1 - \sum_{k\text{-}1}^{N_m} \phi_m \qquad (\cancel{2}1)$$

The ϕ_m values are updated after each time step according to eq. ~~3~~2, where *t-1* indicates the parameter value of the previous time-step, Δt is the time step length (s), V_m the molar volume of the mineral (m^3/mol) and R_m the mineral reaction rate (mol/m^3/s). Rate equations follow the Transition State Theory (Lasaga 1998) and are calculated according to eq. ~~4~~ 3 where A_m is the mineral surface area (m^2/m^3_{rock}), k_{25}, the reaction rate constant (mol/m^2/s) at 25ºC, R is the gas constant (8.3144 J/mol/K), E_a is the activation energy (J/mol), T is temperature (K), a_i^{ni} is the term describing the effect of species i on the rate, and $f_m(\Delta G)$ is the function describing the dependence of the rate on the solution saturation state (Soler 2013). This function is calculated with eq. ~~5~~ 4 where IAP is the ionic activity product of the solution with respect to the mineral, K_{eq} is the equilibrium constant of that mineral, and m_1, m_2 and m_3 are

empirical parameters defining the shape of this function (assumed to be equal to 1 if no experimental data are available).

$$\phi_m=\phi_{m,t-1}+V_m(R_m\Delta t) \qquad (\cancel{3}2)$$

$$R_m=A_m \sum_{\text{terms}} k_{25} e^{\frac{-E_a}{R}\left(\frac{1}{T_{25}}-\frac{1}{T}\right)} \left(\prod_i a_i^{n_i}\right) f_m(\Delta G) \qquad (\cancel{3}4)$$

$$f_m(\Delta G)=\left[1-e^{\left(m_2\left(\ln\frac{IAP}{K_{eq}}\right)^{m_3}\right)}\right]^{m_1} \qquad (\cancel{5}4)$$

The mineral surface area (A_m) is calculated according to eq. ~~6~~ 5 where, $A_{specific}$ is the mineral specific surface area (m^2/g) and MW_m, the mineral molecular weight (g/mol).~~-~~ A threshold mineral volume fraction value must be provided for secondary minerals not initially present in the system to calculate the bulk surface area until the computed time-evolving volume fraction exceeds the threshold value.

$$A_m=\frac{\varnothing_m A_{specific} MW_m}{V_m} \qquad (\cancel{6}5)$$

Activity coefficients for aqueous species are calculated according to the extended Debye-Hückel equation (Steefel 2009). ~~For more detailed information on CrunchFlow, the reader is referred to the user's manual that can be found in www.csteefel.com.~~

The physical system chosen to conduct the reactive transport model is a 1D column of 88 m length representing the laterite profile. In the model, rainwater flows from top to bottom. ~~-~~The column is discretized into a mesh of 250 elements of 0.35 m length each. Models are run for 10^6 years, with a maximum time step of 1 year.

Meteoric water has a constant composition (Table 1~~2~~), ~~from a~~ typical of rainwater from~~of~~ tropical areas (Veneklaas 1990; Williams et al. 1997; Bertolo et al. 2006). It has an ionic strength of 1.4×10^{-4} mol/L. pH has been set ~~equal~~ to 4.5, accounting for both the acidic pH of rainwater and the acidity generated in soils due to the formation of organic acids as a consequence of ~~fter o~~organic matter decomposition (Soler and Lasaga, 1996). Rainwater is flowing along the column at a constant rate during ~~the~~ modeling ~~time~~. The average annual rainfall at Moa ~~(Cuba)~~ in the period 1900-2009 is 1360 mm, of which 990 mm fall during the two wet seasons (data from ~~Climate Change climatic portal,~~ http://sdwebx.worldbank.org/climateportal).

This value agrees with the values between 900 and 1800 mm/y reported by Butt and Cluzel (2013) as summer rainfall for laterite deposit in Caribbean areas. Assuming ~~a~~ retention by the soil of 15% (~~between 12 and 18% as proposed by~~ Veneklaas, ~~(~~1990~~)~~) the infiltration flow rate is 1156 mm/y (4.0×10^{-8} $m^3/m^2/s$).

Neither dry periods nor changes in the infiltration rate are considered during the modeling. Transport is mainly advective. A water diffusion coefficient for solutes of 1.0×10^{-10} m^{-2} s^{-1} is ~~consider~~used and dispersivity is assumed to be equal to 1 m based on the length of the domain (~~83~~ 88 m). Diffusive~~on~~ and dispersive transport ~~are~~ is not significant. ~~There is no lateral flow of water.~~

~~3.2~~ Geochemical system

Initially, the system has a homogeneous mineralogical composition, representing the partially serpentinized peridotite (Table ~~3~~2). Initial mineral volume fractions are based on ~~the~~ field observations ~~done~~ in the Punta Gorda laterite deposit (M10 sample in Fig. 2b). An initial porosity of 12 % is used ~~has been considered~~ to account for the fracture porosity. ~~associated to fractures trough which water flows.~~ En_{90} and Fo_{90} are chosen as representative of the pyroxene and olivine ~~minerals~~ from the unaltered peridotite ~~samples studied~~, respectively.

Initial porewater composition is calculated to be in equilibriun with this set of minerals (Table ~~2~~1). It has an ionic strength of 1.1×10^{-4} mol/L. K and Na are found as free ions, Si is forming ~~the~~ aqueous ~~species~~ H_4SiO_4 (68%) and $H_3SiO_4^-$ (32%). The most abundant aqueous species of carbonate at pH 9.5 is HCO_3^- (86%) although CO_3^{2-} is also significant (13%), together with minor amounts of $MgCO_3$(aq) and $FeCO_3$(aq) (<1%). All iron is found as Fe(II), and is present as Fe^{2+} (50%), $FeOH^+$ (48%) and $Fe(OH)_2$(aq) (2%). Mg aqueous speciation is dominated by Mg^{2+} (99%) although a small amount of $MgOH^+$ (1%) is ~~also observed~~computed. Finally, the main Ni aqueous species are $Ni(OH)_2$ (83%), Ni^{2+} (9%) and $NiOH^+$ (8%).

Besides the primary minerals considered in the initial composition, serpentine II and goethite are included in the calculations and are allowed to precipitate in the case where ~~that~~ porewater is saturated~~s~~ with respect to those minerals. Although several compositions for serpentine II are available (Online resource 1~~Table 1~~), only one composition ~~has been considered~~was used in the model for ~~the~~ sake of simplicity. In the Reference case, the ~~selected~~ composition is set to ~~has been~~ $Mg_{2.798}Fe_{0.102}Ni_{0.049}Si_2O_5(OH)_4$ but the effect of different compositions has been studied in ~~additional~~ sensitivity analyses~~cases~~.

In many oxide deposits ~~the presence of~~ abundant secondary silica has been observed in the form of chalcedony or quartz (Butt and Cluzel 2013). In the model presented here, the saturation index of quartz is monitored and the formation of quartz is ~~further~~ considered in a sensitivity analysis~~case~~.

Moore et al. (2012) highlighted the role of ~~the~~ weathering of silicate mineral as a sink for atmospheric CO_2(g). M~~In fact, m~~agnesite deposits associated to serpentine bodies have been reported (Foster and Eggleton 2002; Ulrich et al. 2014; Quesnel et al. 2016). However, magnesite precipitation, although thermodynamically stable, is inhibited in near surface environments given the strong hydration shells that form around Mg^{2+} ions (Power et al. 2013; Morgan et al. 2015). In these conditions, Königsberger et al. (1999) suggested that hydrated magnesium carbonate minerals, such as nesquehonite ($MgCO_3 \cdot 3H_2O$) form instead. Power et al. (2013) reported that CO_2(g), in turn, may affect the weathering rate of silicate mineral. In order to elucidate the effect of CO_2 in the formation of this type of deposits, the saturation index of nesquehonite is monitored and the effect of different CO_2(g) concentrations is considered in sensitivity analysis~~cases~~.

~~3.3~~ Thermodynamic and kinetic data

Thermodynamic data used in the calculations for aqueous species and for the dissolution/precipitation of quartz and goethite ~~come from~~are from ThermoChimie v.9 database (Giffaut et al. 2014~~),~~ ~~www.thermochimie-tdb.com)~~.

The total list of solute species included in the simulations is shown in Online resource 2. ~~H^+, CO_3^{2-}, O_2(aq), Cl^-, Fe^{2+}, $H_4(SiO_4)$ (aq), K^+, Mg^{2+}, Na^+, Ni^{2+}, OH^-, CO_2(aq), HCO_3^-, $MgHCO_3^+$, $NaHCO_3$(aq), $FeCO_3OH$(aq), $MgCO_3$(aq), $NaCO_3^-$, $NiCO_3$(aq), $NiHCO_3^+$, $Fe(CO_3)_3^{3-}$, $FeHCO_3^+$, $FeCO_3$(aq), $FeCO_3OH^-$, $Ni(CO_3)_2^{2-}$, $Fe(CO_3)_2^{2-}$, $FeOH^+$, $Fe(OH)_2$(aq), $Fe(OH)_3^-$, $Fe(OH)_4^{2-}$, Fe^{3+}, $FeOH^{2+}$, $Fe(OH)_2^+$, $Fe(OH)_3$(aq), $Fe(OH)_4^-$, $FeH_3SiO_4^{2+}$, $Fe_2(OH)_2^{4+}$, $Fe_3(OH)_4^{5+}$, H_2(aq), $MgOH^+$, $Mg_4(OH)_4^{4+}$, $MgH_3SiO_4^+$, $Ni(OH)_2$(aq), $NiOH^+$, $Ni(OH)_3^-$, $Ni_2(OH)^{3+}$, $Ni_4(OH)_4^{4+}$, $H_2SiO_4^{2-}$ and $H_3SiO_4^-$.~~

Solubility constants for En_{90}, Fo_{90}, serpentine I and serpentine II have been modified given that they are not pure magnesium end member minerals. A~~In these cases and for the sake of simplicity, a~~n ideal solid solution between pure end members has been considered for each mineral. For an ideal solid solution $A_{\chi}B_{(1-\chi)}C$, where the pure end members are AC and BC, the solubility constant of a given discrete composition can be calculated using eq. ~~7~~6, where K_{AC} is the solubility constant of pure AC, K_{BC} is the solubility constant of pure BC and χ the molar fraction of A in the solid solution.

$$K=(K_{AC}\chi)^{\chi}\left(K_{BC}(1-\chi)\right)^{1-\chi} \qquad (\cancel{7}6)$$

The pure end members considered for Fo_{90} are fayalite (Fe_2SiO_4), forsterite (Mg_2SiO_4) and the phase Ni_2SiO_4; for En_{90}, the pure end members are enstatite ($MgSiO_3$) and ferrosilite ($FeSiO_3$). In the case of

serpentine I the pure end members are lizardite ($Mg_3Si_2O_5(OH)_4$), népouite ($Ni_3Si_2O_5(OH)_4$) and greenalite ($Fe_3Si_2O_5(OH)_4$) while in the case of serpentine II, Fe(III)-lizardite ($Fe_2Si_2O_5(OH)_4$) is considered instead of greenalite to account for the difference of the valence state of Fe in the octahedral site. ~~between these two serpentines.~~ The log K values of these pure end members are taken from ThermoChimie v.9 when available. ~~However, as this database does not provide data for all of them,~~ A~~a~~dditional log K values~~data are selected from other databases~~ (e.g. forsterite) ~~,~~ are calculated ~~in this study~~ from ~~published~~ ΔG_r^o ~~(e.g. Ni_2SiO_4)~~ or ~~estimated~~ ΔG_f values ~~(e.g. Fe(III) lizardite, Villanova-de-Benavent et al. 2016a)~~from literature (Villanova-de-Benavent et al. 2016a). Selected log K values for pure end-members are ~~shown~~ listed in Table ~~4~~3, whereas~~.~~ log K values calculated for the solid solutions are ~~listed~~ in Table ~~5~~4.

In CrunchFlow, dissolution/precipitation of minerals is ~~always~~ kinetically controlled. As dissolution and/or precipitation of serpentine I, serpentine II, goethite and magnetite is considered to occur under local equilibrium, the rates for these minerals have been modified in order to rapidly achieve equilibrium (large surface areas and/or large rate constants). The threshold volume fraction considered is 10^{-8} and10^{-4} for goethite and serpentine II, respectively.

Dissolution rates for Fo_{90} and En_{90} are assumed equal to those for pure forsterite and enstatite reported in Palandri and Kharaka (2004). ~~and shown in eq.8 and eq.9 respectively, where R is the gas constant (in kJ K^{-1} mol^{-1}), T the temperature (in K) and Ω the mineral saturation ($\Omega = IAP/K_{eq}$). m_1, m_2 and m_3 of eq. 5 are considered equal to 1.~~

$$\cancel{rate\left(mols_{Mg_{10}Si_5O_{20}}\ m^{-2}s^{-1}\right)=\frac{1}{5}\left(10^{-6.85}\times e^{\frac{-67.2kJ/mol}{R}\left(\frac{1}{T}-\frac{1}{298.15K}\right)}\times a_{H^+}^{0.47}+10^{-10.64}\times e^{\frac{-79kJ/mol}{R}\left(\frac{1}{T}-\frac{1}{298.15K}\right)}\right)\times\left(1-\Omega\right)\quad(8)}$$

$$\cancel{rate\left(mols_{Mg_{10}Si_{10}O_{30}}\ m^{-2}s^{-1}\right)=\frac{1}{5}\left(10^{-9.02}\times e^{\frac{-80kJ/mol}{R}\left(\frac{1}{T}-\frac{1}{298.15K}\right)}\times a_{H^+}^{0.60}+10^{-12.72}\times e^{\frac{-80kJ/mol}{R}\left(\frac{1}{T}-\frac{1}{298.15K}\right)}\right)\times\left(1-\Omega\right)\quad(9)}$$

The assignment of a value for the reactive area of forsterite and enstatite is not straightforward. Dissolution rates measured in the laboratory are ~~from~~ 2 to 5 orders of magnitude faster than in field due to a variety of factors such as the presence/absence of inhibitors or catalyzers such as ~~(e.g.~~ organic acids~~)~~, hydrologic regimes, armoring of natural surfaces or the affinity of secondary minerals (Navarre-Sitchler et al. 2011) ~~and the way how the specific surface for calculating the rates of dissolution of different minerals in a model has yet to be solved (Sokolova 2013)~~. After preliminary calculations, a reactive area of 0.0005 m^2/g for Fo_{90} and of 0.005 m^2/g for En_{90} is considered in the model. These values g~~a~~ive results

comparable to field observations. Nevertheless, the effect of higher surface areas~~ (and thus, higher dissolution rates),~~ is studied in ~~additional~~ sensitivity analyses~~cases~~.~~-~~ Mn- oxyhydroxides have not been considered.

The Ni content in the goethite from ~~of~~ Punta Gorda ranges from 0.8 to 4.0 wt.% Ni. In the model presented here, this Ni is sorbed onto the goethite surface. Assuming that when the Ni content is 4.0 wt.% all surface sites are occupied by Ni, the maximum sorption capacity of goethite can be calculated, being 6.5 sites/nm^2 for a surface area of 65.2 m^2/g. This value is consistent with the values proposed by Davis and Kent (1990) (2.6-16.8 sites/nm^2 for Fe oxyhydroxides), or Hayes and Leckie (3-11 sites/nm^2). Information concerning the sorption of Ni onto goethite is scarce (Marcussen et al. 2009; Rajapaksha et al. 2012). Sorption of Ni onto the goethite surface is modeled following a one-site non electrostatic sorption model based on~~in the model proposed in~~ Marcussen et al. (2009) (Table ~~6~~5), where Ni sorbs onto goethite surface forming the surface complex >Fe_ONi$^+$. These authors used a log K for goethite surface protonation/deprotonation from Richter et al. (2005) but an update of these values (Richter and Brendler 2008) is used in ~~this model~~our study. The original log K values were provided for a density site of 2.31 sites/nm^2 and they have been recalculated to account for the site density of Punta Gorda goethite according to eq. 7~~10~~ (Richter et al. 2005), where K are the sorption equilibrium constants, Γ the site density (sites/nm^2), and the subscript *o* stands for the new values calculated for 6.5 sites/nm^2. Total sorption capacity of goethite is 0.0625 moles sites/moles goethite.

$$\log K_o = \log K + \frac{\Gamma}{\Gamma_o} \qquad (7\cancel{10})$$

~~4~~ Results and discussion

The modeling results~~exercise~~ presented in this paper consists of a Reference case whose initial and boundary conditions have been detailed above and a set of Sensitivity ~~cas~~analyses in which some parameters have been modified with respect to those of the Reference case. ~~in order to evaluate the effect of their uncertainty in the results.~~

~~4.1~~ Reference case

The residence time of water in the profile is 2.7 years. This residence time is very short compared to the total time of modeling (10^6 years) and indicates, as expected, that the influence of the initial porewater composition on the final results can be neglected.

Fig. 4 shows the evolution of the mineral composition (% wt), sorbed Ni concentration, and porosity as a function of depth at different elapsed times. When looking at Fig. 4 the reader must take into consideration ~~remember~~ that the weight percentage of a given mineral can increase either because of its precipitation or because of the dissolution of other minerals without precipitation.

~~As explained previously and i~~In order to simulate the effect of unsaturated flow, once the model run starts, porewater is equilibrated with atmospheric O_2(g) and CO_2(g) all along the profile. Due to ~~the availability of~~ O_2(g) equilibrium, ~~some immediate changes are observed in the initial mineral composition of the profile. M~~magnetite becomes unstable and is transformed into goethite, ~~some~~ serpentine II precipitates, and porosity decreases before 1000 years of elapsed time to values down to 5% (Fig. 4). Although this is realistic ~~to occur here~~, changes at the bottom of the weathering profile are ~~clearly~~ an artifact caused by the assumption of equilibrium with atmospheric O_2(g) and CO_2(g). Given the impossibility of fixing a realistic depth in which the system changes from unsaturated to saturated conditions, we have carried out the *Less_carb* sensitivity case in which only the infiltrating rainwater (not along the profile) is in equilibrium with atmospheric O_2(g) and CO_2(g).

During the first 1000 years, two different reactions are observed to occur in the profile. Dissolution of En and Fo occurs ~~in~~ all along the profile, while precipitation of Srp I and Srp II occurs ~~in all~~along the profile, except at the top. ~~As Srp I and Srp II react at equilibrium,~~ pH is buffered to 8.6 (Fig. 5) and Ni aqueous concentration is ~~very~~ low ($<10^{-15}$ mol/L). The main species occupying the goethite surface is >FeOH (>95%).

However, at the top of the profile, where rainwater is acidifying the system, Srp I dissolves together with Fo_{90} and En_{90} and the saprolite horizon begins to develop. Srp II and goethite precipitate removing Ni and Fe from solution. In fact, the amount of Srp II precipitating depends on the amount of Ni released from the dissolution of Fo_{90} and Srp I. Fe released by En_{90}, Fo_{90} and Srp I that has not been incorporated into Srp II, precipitates as goethite. The presence of both Srp I and Srp II ~~still~~ buffers pH at a value of 8.6 and causes~~keeps~~ Ni aqueous concentration remain at ~~to~~ very low values. Goethite surface speciation is dominated by >FeOH.

~~Formation of Srp II occurs while either Srp I or Fo_{90} dissolve as they are the primary minerals providing Ni to the system.~~ Between 1000 and 10000 years of elapsed time, no significant changes are observed, except that~~-~~, at the top of the profile, Srp I has been exhausted. As a consequence, porosity has significantly increased. However, as Fo_{90} and En_{90} are still in the system, they dissolve and Srp II and

goethite precipitate. Although in the model Fo_{90} is the first silicate mineral to dissolve followed by En_{90}, as observed by Freyssinet et al. (2005), Golightly (2010) and Hewawasam et al. (2013), their coexistence with Srp II and Gth without Srp I is not in agreement with the paragenesis observed in the field in which neither enstatite nor forsterite are in contact with Srp II. ~~As will be discussed later in the *Rate* sensitivity case (in which En_{90} and Fo_{90} dissolve faster), one~~ One of the most uncertain parameters in reaction kinetics is the choice of reactive area, which suggests ~~. The results observed here let us think~~ that the reactive areas used in th~~is~~e Reference case could be too low. In any case, ~~it is worth to say that~~ this is a transitory effect that is not observed after 10^6 years of elapsed time.

B~~Moreover, also b~~etween 1000 and 10000 years of elapsed time, a new horizon starts to develop in the model first node, in contact with the infiltrating rainwater. The precipitation of goethite has increased its sorption capacity and causes the dissolution of Srp II because Ni is preferentially sorbed onto the goethite surface (>FeONi$^+$). pH decreases from 8.6 to a buffered value of 8.3.~~, where it remains buffered.~~ Ni aqueous concentration is close to 10^{-8} mol/L.

During the period 10^4 – 10^5 years, two significant observations can be made. On one hand, Fo_{90} is exhausted~~ out the system~~, which means that the only processes controlling Ni concentration in solution are the formation of~~ Srp I or~~ Srp II and the sorption of Ni onto goethite surface. On the other hand, a new ~~horizon (~~oxide horizon~~)~~ is starting to form at the top of the profile because Srp II has been dissolve ~~exhaust~~ed. pH is no longer buffered at 8.3. Enstatite is dissolving ~~and provides~~yielding Fe that precipitates as goethite. As a consequence, the porosity increases up to 75%. The formation of >FeONi$^+$ displaces H^+ from the goethite surface (Table ~~6~~5) and contributes to the decrease of pH together with the input of acidic water. Ni aqueous concentration is about 3×10^{-7} mol/L.

At 10^5 years of elapsed time, the three main horizons of a typical laterite profile ~~can already be identified~~have formed (Fig. 4). At the top of the column, there is the goethite-dominated horizon; below 10 m depth, Srp I is in equilibrium with Srp II and Gth at pH 8.6 in a~~(~~ partially weathered peridotite horizon,~~)~~ and between both layers, there is a narrow horizon in which serpentine II is in equilibrium with a goethite with Ni sorbed, the ~~(~~saprolite horizon~~)~~ (Fig. 4).

From 10^5 years on, slight changes are ~~observ~~predicted. The oxide and saprolite horizons develop and ~~displace~~ the interfaces are displaced towards greater depths. A~~It is worth to say that a~~t the top of the profile, ~~as~~ there is no more forsterite providing Ni to the system and the pH is acid, such that desorption of Ni ~~is promoted,~~ increases~~ing~~ Ni aqueous concentration. At 4×10^5 years of elapsed time, enstatite is

exhausted and goethite becomes the only phase in this horizon. pH is 4.5 and porosity is ~~very~~ high, about 91% (Fig. 4). Ni released from the goethite surface is sorbed downflow on the goethite in the saprolite horizon until its surface is saturated~~s~~ (at 8×10^5 years of elapsed time). From this moment, saprolite horizon develops faster given that no more Ni can sorb onto goethite and it is available for serpentine precipitation.~~.~~

The model results obtained ~~in the model~~ agree with the laterite formation rates reported in literature. In 10^6 y, the thickness of weathered laterite might be 10-20 m (Freyssinet et al. 2005), 29-58 m (Golightly 2010) or 2-75 m (Hewawasam et al. 2013). Hewawasam et al. (2013) observed that in Sri Lanka laterites, weathering processes are occurring at the reaction front, and are displaced towards greater depths as minerals become ~~totally~~ weathered. According to Goodfellow et al. (2011) this is because weathering reactions are inhibited in those areas where porewater is saturated with respect to weathering products that is, far from the water table, and ~~by cont~~in contrast~~rary~~, weathering ~~processes are~~is enhanced in the vadose zone. In agreement with those authors, in the model presented here, the reaction front starts at the top of the profile and is moving downward with time as weathering reactions ~~occur~~progress.

The model satisfactorily explains the formation of the three different horizons observed in the field in a period of time around 10^6 y. The first one, with a thickness~~width~~ of 61 m, is ~~located~~ at the top of the profile and is composed of goethite. In this horizon, the porosity is ~~very~~ high (Fig. 4), porewater composition is ~~very~~ poor in Mg, Si, Fe and Ni, pH is around 4.5 and the goethite surface is saturated with H^+ (Fig. 6).

The second horizon is formed by goethite and serpentine II. It has a thickness of 11 m with an average porosity of 40%, although it increases at the bottom. pH increases up to 8.3 and goethite contains up to 4 wt.% Ni sorbed onto its surface. ~~>Fe_ONi$^+$ is the~~ The main surface species is >Fe_ONi$^+$. (Fig. 6). In this saprolite horizon, the ratios between Mg/Si and CO_3/Mg in solution are 1.4 and 2.0 respectively, in agreement with the observations of Golightly (1981). pH values also agree with those reported for saprolite horizons (Golightly 1981, 2010; Pelletier 1996).

Another similitude with field observations is the difference between the development of the limonitic and saprolite horizons. The ~~is~~ larger thickness of the limonitic horizon in relation to that of saprolite has been observed in areas with maximum lixiviation (Butt and Cluzel 2013~~)~~), and unsaturated conditios, i.e. porewater in equilibrium with atmospheric ~~as the one considered in the model, where despite assuming saturated conditions,~~ O_2(g) and CO_2(g) ~~are available throughout the column~~. Nevertheless, the goethite

horizon is significantly thicker (61 m) than the saprolite horizon (11 m), ~~but this is~~ due to the fact that ~~code capabilities as~~ the model does not take into account ~~for~~ the collapse of this horizon. In case of collapsing, the thickness of the goethite horizon will be smaller and similar to that observed in the Punta Gorda deposit ~~at Moa Bay area (~~(30m, Fig. 1).

The third and deepest horizon, with a depth limited by model dimensions, represents a partially weathered serpentinized peridotite, with serpentine I in equilibrium with serpentine II and goethite. pH is 8.6 and Ni is not sorbed onto goethite (Fig. 6). Porosity is ~~very~~ low, close to 5%.

After 10^6 y, 76% of Mg and 80% of Si have been leached from the profile, in agreement with observations reported in Golighlty (1981) and Butt and Cluzel (2013) (RC in Fig. 7). A significant increase of Mg aqueous concentration is observed between the goethite and saprolite horizons. Fe and Ni are scarcely leached out of the system.

The model results suggest ~~obtained confirm~~ that sorption of Ni onto the goethite surface can explain the amount of Ni found in the goethite at Moa. In the model, however, sorption of Ni occurs only ~~in the~~on goethite in contact with serpentine II. This distribution, in accordance with the observations of Dublet et al. (2015) of a regular decrease in bulk Ni content upwards in the profile and of Soler et al. (2008) in the goethite horizon of Loma de Hierro deposit, is directly linked to the evolution of pH. Sorption of Ni onto goethite depends on pH, and as can be seen in Fig. 6, when pH decreases below 7, sorption of Ni significantly decreases achieving values around 10% or less at pH 5 (Dublet et al. 2015). In natural conditions, however, goethite particles with Ni sorbed onto their surface might flocculate or form aggregates. For goethite, the point of zero charge (PZC) is between pH = 6.5 to 9.5 (Strauss et al. 1997; Gaboriaud and Ehrhardt, 2002). At the PZC, a dispersion of particles exhibits its maximum flocculation rate. In the profile, this range of pH is encountered in the saprolite, towards the limonitic horizon, where it might well favor the flocculation/aggregation of the goethite particles that could prevent desorption of Ni. In the model, nesquehonite is always subsaturated (saturation indices below -2) while quartz presents saturation indices about 0.7 in the partially serpentinized peridotite horizon and close to 0.4 in the saprolite horizon.

~~4.2~~ Sensitivity ~~cas~~analyses

Different ~~sensitivity~~ cases have been investigate~~calculate~~d to evaluate the effect of the uncertainty of some key parameters on the model results. As ~~can be seen~~shown ~~in~~ in Table ~~Table 7~~6, ~~where the~~

~~differences between these sensitivity cases and the Reference case (RC) are highlighted,~~ sensitivity analys~~eas~~es explore the effect of not considering sorption of Ni onto goethite (*No_ads* case), of using different chemical compositions for serpentine II (*Srp II** and *Srp II*$^{\$}$ cases), of considering faster dissolution rates of Fo_{90} and En_{90} (*Rate* case), of considering a smaller carbonate concentration (*Less_carb* case), ~~and of~~ or allowing the precipitation of quartz (*Qt* case).

In the ***No_ads*** sensitivity ~~case~~analysis, the formation of surface species onto goethite is not considered. After 10^6 years of elapsed time, the same horizons developed as in the RC, with a goethite horizon with pH 4.5, a saprolite horizon with serpentine II and goethite at pH 8.3, and a partially weathered peridotite with serpentine I and II and goethite at pH 8.6. ~~, are also obtained.~~ Mg and Si are also significantly leached (Fig. 7)~~;~~ but as shown ~~een~~ in Fig. 8, the saprolite horizon is thicker than in the RC. This is due to the fact that, on one hand, all Ni is available to precipitate in Srp II whereas ~~(~~in RC, sorption of Ni was dominant and Srp II formed once the goethite surface was saturated~~)~~, and on the other, the pH of porewater is not affected by the (de)protonation of goethite. In the RC, pH was lower in the saprolite horizon because sorption of Ni displaced H^+ from the goethite surface, while in the *No_ads* case, the pH in the saprolite horizon is maintained at 8.3, the same pH that is achieved in the RC when goethite becomes saturated in Ni (Fig. 9).

To account for the variability of compositions of Srp II observed in the field, two more chemical compositions ~~of Srp II~~ have been used in the sensitivity ~~cases~~ analyses ***Srp II**** and ***Srp II***$^{\$}$ (Table ~~5~~4). These two Srp II have been chosen as they are the compositions having the lowest and the highest solubility constants, respectively. Results indicate that the same main processes are occurring ~~are the same~~ as in the RC (Fig.7, Fig. 9), but that the composition of Srp II ~~has effectively some e~~affects ~~on~~ the final distribution of the profile horizons (Fig. 8). On one hand, the thickness of the saprolite horizon, dominated by Srp II, decreases as the solubility of this mineral increases (*Srp II*$^{\$}$ in Fig. 8). On the other hand, the amount of leached Ni is higher in the sensitivity case *Srp II**, that is, the one considering the Srp II with the lowest ~~poorest in~~ Ni content (Table ~~5~~4).

In~~As already mentioned when discussing the RC results, in~~ the ***Rate*** case**,** the reactive areas of Fo_{90} and En_{90} are set equal to 0.1 m^2/g to obtain dissolution rates of Fo_{90} and En_{90} that are 200 and 20 times faster, respectively, than in the RC. Results show that these faster dissolution rates increase the amounts of Si, Ni, Mg and Fe released, which also leads to increased goethite precipitation and Ni adsorption. Fo_{90} and En_{90} are completely consumed before (1000 and 1.5×10^5 years respectively), without further effects on

~~and therefore, their control on~~ laterite formation. ~~finishes soon.~~ After 10^6 years of elapsed time, differences with the RC are minor (Fig. 7-9).

In the sensitivity ~~case~~ analysis ***Less_carb***, only the infiltrating rain water ~~at the inlet~~ is in equilibrium with atmospheric O_2(g) and CO_2(g). ~~By doing this change, t~~The model reproduces a case in which the system is fully saturated (water table at the surface), limiting the input of O_2(g) and CO_2(g) to the system (Butt and Cluzel 2013). As ~~can be seen~~shown in Fig. 8, the advancement of the weathering front after 10^6 years is ~~very~~ small compared to the RC. The main reason for such big difference is the availability of carbonate, which affects pH. In this sensitivity analysis~~case~~, the lack of dissolved CO_2(g) ~~(a weak acid)~~ does not buffer pH and, as a result of Srp I dissolution, pH goes up ~~very~~ quickly and the solution becomes saturated~~s~~ with respect to primary minerals (Fig. 8). In the RC, where atmospheric CO_2(g) is always available in the column, dissolution of CO_2(g) provides enough acidity to buffer the increase in pH caused by silicate mineral dissolution. This observation agrees with Golightly (1981) that identified carbonate as one of the principal agents of weathering. When carbonate is not available, the solubility of serpentine~~s~~ is lower and the reaction front moves slowly. As a consequence, in 10^6 years of elapsed time, Mg and Si leaching is not as important as for ~~equivalent to~~ the other cases (Fig. 7) and pH is around 10 (Fig. 9). The *Less_carb* and RC results suggest that the aqueous carbonate concentration is, in fact, an important key parameter controlling the rate of laterite formation. Any phenomena preventing CO_2(g) equilibration with porewater would lessen laterite profile development.

As reported previously in the RC, saturation indices of quartz indicated a slight oversaturation, especially along the saprolite and peridotite horizons. In the ***Qt*** sensitivity ~~case~~analysis, quartz is allowed to precipitate ~~in case it oversaturates~~ according to local equilibrium. Results show that quartz precipitation is significant because Si is preferentially retained as quartz rather than being incorporated in Srp II and, consequently, the weathering front is advancing faster. After 10^6 years of elapsed time, the profile presents two different horizons (Fig. 8). The first 11.5 m are of goethite, with a porosity of 91% and a pH of 4.5; and the other 75 m are composed of 43% (in vol.) of quartz and 9 % (in vol.) of goethite with a porosity of 48% and a pH of 6 (Fig. 9). All Mg and nearly 40% of Ni have been leached from the system, while leaching of Si is reduced to 15% (Fig. 7). ~~-~~Microcrystalline quartz in laterite profiles has been reported in some profiles (e.g. Golightly 1981; Tauler et al. 2009; Villanova-de-Benavent et al. 2014) and observed ~~to occur~~ in ~~some~~ cases with small lixiviation rates (Butt and Cluzel 2013), but it does not form in those cases where weathering rate is fast (Golightly 2010). In the RC, quartz saturation indicates~~d~~ its

possible precipitation but the results obtained when quartz is allowed to precipitate are not consistent with field observations. An explanation to this might be found in the value of the saturation indices calculated for quartz, that were not higher than 0.7~~6~~. These small saturation indices might not be enough to overcome a kinetic barrier for~~allow~~ the precipitation of quartz. Instead of the precipitation of quartz under local equilibrium, the precipitation of an~~ more~~ amorphous phase such as SiO_2(am), or a kinetically controlled~~ limited~~ precipitation of quartz should have been ~~-~~considered.

~~5.~~ Conclusions

This paper presents a reactive transport model of the formation of the Punta Gorda Ni~~-~~-laterite deposit of Moa mining district (northeast of Cuba). The model is based on the ~~direct formation~~ conceptual model ~~described in~~of Butt and Cluzel (2013), according to which laterite deposits form due to a continuous weathering of a partially serpentinized peridotite under tropical climate. Numerical model considers a 1D column of 88 m length initially composed of Fo_{90}, En_{90}, Srp I and Mag. Due to the interaction with rainwater, these primary minerals dissolve, and a Fe(III) and Ni bearing serpentine (Srp II) and goethite ~~are left to~~ precipitate. Ni is allowed to sorb onto goethite. ~~Models are run for 10^6 y.~~

Although some of the assumptions made in the numerical model are~~ a~~ simplifications of the real system, results of the model are consistent with ~~validate~~ the conceptual model about the formation of oxide type Ni-laterite ~~this kind of~~ deposits:

- After 10^6 years of elapsed time, simulations reproduce the three main horizons observed in the field: a) a thick limonite horizon,~~, placed~~ at the top of the profile, composed of goethite, b) a narrow saprolite horizon, in the middle, composed of Srp II and Gth, and c) a partially weathered serpentinized peridotite horizon, at the bottom, in which Srp~~serpentine~~ I, ~~serpentine~~Srp II and ~~goethite~~Gth coexist.
- Simulations show the increase of porosity from values close to 5% at the bottom to values close to 90% at the top of the profile, due to the dissolution of silicate minerals ~~(collapse of limonite horizon is not simulated)~~ and the pH increase from 4.5 at the top (rainwater pH) to values close to 8.6 at the bottom, being 8.3 at the saprolite horizon.
- Sorption of Ni onto goethite can explain the field observations. Ni sorption onto goethite is linked to pH~~ profile~~, showing its maximum in the ~~at~~ saprolite horizon~~profile~~, as observed in the field. Sorption onto goethite in the limonite horizon decreases because of the acidic pH, which displaces

Ni^{2+} from the surface sites. In the serpentinized peridotite horizon, sorption is negligible because Ni is preferentially retaine~~locate~~d in Srp I.

- During the laterization process, Mg and Si are leached out the system, while Fe and Ni are conserved.

This simulation exercise has been useful not only to identify but also, to quantify, the effect that some variables can have on the formation of laterites:

- The saprolite reaction front does not advance while there is Srp I in the system.
- Protonation/desprotonation of goethite surface exerts a significant control on porewater pH as it increases acidic pH of entering rainwater but also decrases pH of saprolite horizon porewater to values below 8.3, preventing the development of saprolite horizon. Nevertheless, this control finishes when goethite surface sites saturate.
- Aqueous carbonate concentration is an important key parameter as it controls the rate of laterization process, ~~being faster as higher the concentration is~~with laterization increasing with carbonate concentration. This is due to carbonic acid buffering capacity, which buffers the increase of pH due to silicate dissolution.
- Forsterite is the main mineral providing Ni to the system. The dissolution rate ~~at which it dissolves but also~~of Fo and ~~the rate of~~ En ~~enstatite dissolution~~ affects the thicknesses of the different horizons.
- Serpentine II composition influences the development of laterite profile, from two perspectives: ~~a~~ serpentine II poor in Ni causes an increase of the % of Ni leached after 10^6 years of elapsed time and since composition determines the solubility constant of serpentine, the more soluble the serpentine is, the narrower the saprolite horizon is. In any case, its effect is minor and must be further evaluated.
- Precipitation of quartz significantly enhances the formation of the limonitic horizon and inhibits the formation of the saprolite horizon. The inclusion of quartz or even an amorphous silica phase must be ~~further~~ evaluated in more details.

Results of this study ~~paper~~ provide new valuable insights to the understanding of the differences between Ni-laterite deposit types and show the capabilities of reactive transport simulations to test and validate conceptual models.

~~Nevertheless, t~~The model could ~~an still~~ be improved by increasing either the complexity of the geochemical system (more minerals, solid solutions, incorporation of Ni into goethite structure,~~-~~…) or the physical system (2D or 3D, matrix diffusion to simulate corestones structures, mineral heterogeneity…). Finally, investigations on the PZC of goethite under the hydrochemical conditions of the Moa profile would account for flocculation of particles that may preserve Ni all along the goethite horizon.

ACKNOWLEDGEMENTS

This research has been financially supported by FEDER Funds, the Spanish projects CGL2009-10924 and CGL2012-36263 and Catalan project 2014-SGR-1661. We are grateful to Prof. J.P. Golightly, Prof. G.Beaudoin, -M.Cathelineau and an anonymous reviewer for their careful reviews and constructive criticism of the original manuscript.

Conflict of interest

The authors declare that they have not conflict of interest.

References

Aiglsperger, T., Proenza, J.A., Lewis, J.F., Labrador, M., Svojtka, M., Rojas-Purón, A., Longo, F., Ďurišová, J. (2016): Critical metals (REE, Sc, PGE) in Ni laterites from Cuba and the Dominican Republic. Ore Geol Rev 73: 127-147. DOI:10.1016/j.oregeorev.2015.10.010

Arai, Y. (2008) Spectroscopic evidence for Ni(II) surface speciation at the iron oxyhydroxides-water interface. Environ Sci Technol: 1151–1156

Beukes JP, Giesekke EW, Elliott W (2000) Nickel retention by goethite and hematite. Miner Eng 13: 1573-1579

Bertolo R, Hirata R, Sracek O (2006) Geochemistry and geochemical modeling of unsaturated zone in a tropical region in Urânia, Sao Paulo state, Brazil. J Hydrol 329: 49– 62

Brunauer S, Emmett PH, Teller E (1938) Adsorption of gases in multimolecular layers. J Am Chem Soc 60: 309-319

Bryce AL, Kornicker WA, Elrerman AW (1994) Nickel adsorption to hydrous ferric oxide in the presence of EDTA: effects of component addition sequence. Environ Sci Technol 28: 2353-2359

Buerge-Weirich D, Hari R, Xue H, Behra P, Sigg L (2002) Adsorption of Cu, Cd, and Ni on goethite in the presence of natural groundwater ligands. Environ Sci Technol 36: 328-336

Butt CRM, Cluzel D (2013) Nickel Laterite Ore Deposits: Weathered Serpentinites. Elements 9:123-128. doi: 10.2113/gselements.9.2.123

Carvalho-e-Silva MLM, Partiti CSM, Enzweiler J, Petit S, Netto SM, De Oliveira SMB (2002) Characterization of Ni-containing goethites by Mössbauer spectroscopy and other techniques. Hyperfine Interact 142: 559–576

Carvalho-e-Silva MLM, Ramos AY, Nogueira Tolentino HC, Enzweiler J, Netto SM, Martins Alves MC (2003) Incorporation of Ni into natural goethite: An investigation by X-ray absorption spectroscopy. Am Mineral 88: 876–882. 0003-004X/03/0506–87605.00 876

Cathelineau M, Quesnel B, Gautier P, Boulvais P, Couteau C, Drouillet M (2016) Nickel dispersion and enrichment at the bottom of the regolith: formation of pimelite target-like ores in rock block joints (Koniambo Ni deposit, New Caledonia) Miner Deposita 51:271-282. doi: 10.1007/s00126-015-0607-y

Corbella M, Ayora C, Cardellach E (2004) Hydrothermal mixing, carbonate dissolution and sulfide precipitation in Mississippi Valley-type deposits. Miner Deposita 39: 344–357. doi: 10.1007/s00126-004-0412-5.

Cornell RM (1991) Simultaneous incorporation of Mn, Ni and Co in the goethite (α-FeOOH) structure. Note. Clay Miner 26: 427-430

Coughlin BR, Stone AT (1996) Nonreversible adsorption of divalent metal ions (Mn^{II}, Co^{II}, Ni^{II}, Cd^{II} and Pb^{II}) onto goethite: effects of acidification, Fe^{II} addition, and picolinic acid addition. Environ Sci Technol 29: 2445-2455

Davis JA, Kent DB (1990) Surface complexation modeling in aqueous geochemistry. In: Hochella MF, White AF (eds) Reviews in Mineralogy, Mineral-Water Interface Geochemistry, 23, Mineralogical Society of America, Washington, DC, pp. 177–260

De Keijser ThH, Langford JJ, Mittemeijer EJ, Vogels ABP (1982) Use of the Voigt function in a single-line method for the analysis of X-ray diffraction line broadening. J Appl Crystallogr : 308-314

Dublet G, Juillot F, Morin G, Fritsch E, Fandeur D, Ona-Nguema G, Brown Jr GE (2012) Ni speciation in a New Caledonian lateritic regolith: A quantitative X-ray absorption spectroscopy investigation. Geochim Cosmochim Acta 95: 119–133

Dublet G, Juillot F, Morin G, Fritsch E, Fandeur D, Brown Jr GE (2015) Goethite aging explains Ni depletion in upper units of ultramafic lateritic ores from New Caledonia. Geochim Cosmochim Acta 160: 1-15

Fan R, Gerson AR (2011) Nickel geochemistry of a Philippine laterite examined by bulk and microprobe synchrotron analyses. Geochim Cosmochim Acta 75: 6400–6415

Fletcher RC, Brantley SL (2010) Reduction of bedrock blocks as corestones in the weathering profile: observations and model. Am J Sci 310: 131–164. doi: 10.2475/03.2010.01

Fletcher RC, Buss HL, Brantley SL (2006) A spheroidal weathering model coupling porewater chemistry to soil thicknesses during steady-state denudation. Earth Planet Sc Lett 244: 444–457.

Fischer L, Brümmer GW, Barrow NJ (2007) Observations and modelling of the reactions of 10 metals with goethite: adsorption and diffusion processes. Eur J Soil Sci 58: 1304–1315. doi: 10.1111/j.1365-2389.2007.00924.x

Foster L, Eggleton RA (2002) The Marlborough nickel laterite deposits. In: Roach I.C. ed. 2002. Regolith and Landscapes in Eastern Australia 33-36. CRC LEME

Freyssinet Ph, Butt CRM, Morris RC (2005) Ore-forming processes related to lateritic weathering: Econ Geol 100th Anniv Vol: 681-722

Galí S, Proenza JA, Labrador M, Tauler E, Melgarejo JC (2007) Numerical modeling og oxide-type Ni laterite deposits: preliminary results. In CJ Andrew et al. (eds) Digging Deeper Proceedings of the ninth bienal SGA meeting. Dublin (Ireland), 1385-1388

Gamsjäger H, Bugajski J, Gajda T, Lemire RJ, Preis W (2005) Chemical thermodynamics of Nickel, Nuclear Energy Agency Data Bank, Organisation for Economic Co-operation and Development, Ed., vol. 6, Chemical Thermodynamics, North Holland Elsevier Science Publishers B. V., Amsterdam, The Netherlands.

Gehring AU, Fischer H, Louvel M, Kunze K, Weidler PG (2009) High temperature stability of natural maghemite: a magnetic and spectroscopic study. Geophys J Int 179, 1361–1371. doi: 10.1111/j.1365-246X.2009.04348.x

Giffaut E, Grivé M, Blanc Ph, Vieillard Ph, Colàs E, Gailhanou H, Gaboreau S, Marty N, Madé B, Duro L (2014) Andra thermodynamic database for performance assessment: ThermoChimie. Appl Geochem 49: 225-236

Gleeson SA, Butt CR, Elias (2003) Nickel laterites: a review. SEG News 54: 11–18.

Goodfellow BW, Hilley GE, Schulz MS (2011) Vadose zone controls on weathering intensity and depth: Observations from grussic saprolites Appl Geochem 26: S36–S39. doi:10.1016/j.apgeochem.2011.03.023

Golightly JP (1981) Nickeliferous laterite deposits. Econ Geol, 75th anniversary volume 710-735

Golightly JP, Plamondon M, Srivastava RM (2008) 43-101F1 technical report on the Camarioca Norte and Camarioca Sur nickel laterite properties in Cuba (www.sedar.com Sherritt International filed May 9 2008).

Golightly JP (2010) Progress in understading the evolution of nickel laterites. Soc Eco Geo Spe Pub 15: 451-485

Golightly JP, Arancibia ON (1979) The chemical composition and infrared spectrum of nickel- and iron-substituted serpentine from a nickeliferous laterite profile, Soroako, Indonesia. Can Mineral 17: 719–728

Hayes KF, Leckie JO (1987) Modeling ionic strength effects on cation adsorption at hydrous oxide/solution interfaces. J Colloid Interf Sci 115: 564-572

Hewawasam T, von Blanckenburg F, Bouchez J, Dixon JL, Schuessler JA, Maekeler R. (2013) Slow advance of the weathering front during deep,supply-limited saprolite formation in the tropical Highlands of Sri Lanka Geochim Cosmochim Acta 118: 202–230.

Klug HP, Alexander LE (1962) X-Ray Diffraction Procedures for polycrystalline and amorphous materials (Chapter 9). New York. John Wiley and Sons. Inc.

Königsberger E, Königsberger LC, Gamsjäger H (1999) Low temperature thermodynamic model for the system Na_2CO_3-$MgCO_3$-$CaCO_3$-H_2O. Geochim Cosmochim Acta 63: 3105-3119

Lambiv Dzemua G, Gleeson S A, Schofield P F (2013) Mineralogical characterization of the Nkamouna Co–Mn laterite ore, southeast Cameroon. Miner Deposita 48: 155-171. DOI 10.1007/s00126-012-0426-3

Langford JL (1978) A rapid method for analyzing the breaths of diffraction and spectral lines using the Voigt function. J Appl Crystallogr 11: 10-14

Lasaga AC (1998) Kinetic Theory in the Earth Sciences. Princeton. University Press, Princeton

Lavaut W (1998) Tendencias geológicas del intemperismo de las rocas ultramáficas en Cuba oriental. Minería y Geología 15: 9–16.

Lebedeva MI, Fletcher RC, Balashov VN, Brantley SL. (2007) A reactive diffusion model describing transformation of bedrock to saprolite. Chem Geol 244: 624–645

Lewis JF, Draper G, Proenza JA, Espaillat J, Jimenez J (2006) Ophiolite-related ultramafic rocks (serpentinites) in the Caribbean Region: A review of their occurrence, composition origin, emplacement and Ni-laterite soils formation. Geol Acta 4: 237-263

Linchenat A, Shirakova I (1964) Individual characteristics of nickeliferous iron (laterite) deposits of the northeast part of Cuba (Pinares de Mayari, Nicaro and Moa). 24th International

Geological Congress, Montreal, Part 14, Section 14, 172–187

Louër D, Aufrédic JP, Langford JL, Ciosmak D, Niepce JC (1983) A precise determination of the shape, size and distribution of size of crystallites in zinc oxide by X-ray line-broadening analysis. J Appl Crystallogr 16: 183-191

Manceau A, Schlegel ML, Musso M, Sole VA, Gauthier C, Petit PE, Trolard F (2000) Crystal chemistry of trace elements in natural and synthetic goethite. Geochim Cosmochim Acta 64: 3643-3661

Marchesi C, Garrido CJ, Godard M, Proenza JA, Gervilla F, Blanco-Moreno J (2006) Petrogenesis of highly depleted peridotites and gabbroic rocks from the Mayarí-Baracoa Ophiolitic Belt (eastern Cuba). Contrib Mineral Petr 151: 717–736

Marcussen H, Holm PE, Strobel BW, Hansen HCB (2009) Nickel sorption to goethite and montmorillonite in presence of citrate. Environ Sci Technol 43: 1122-1127

Moore J, Lichtner PC, White AF, Brantley SL (2012) Using a reactive transport model to elucidate differences between laboratory and field dissolution rates in regolith. Geochim et Cosmochim Acta 93: 235–261

Morgan B, Wilson SA, Madsen IC, Gozukara YM, Habsuda J (2015) Increased thermal stability of nesquehonite ($MgCO_3 \cdot 3H_2O$) in the presence of humidity and CO_2: Implications for low-temperature CO_2 storage. Int J Greenh Gas Con 39: 366–376. doi:10.1016/j.ijggc.2015.05.033

Navarre-Sitchler A, Steefel CI, Sak PB, Brantley SL (2011) A reactive-transport model for weathering rind formation on basalt. Geochim Cosmochim Acta 75: 7644-7667 doi:10.1016/j.gca.2011.09.033

Oliveira SMB, Partiti CSM, Enzweiler J (2001) Ochreous laterite: a nickel ore from Punta Gorda, Cuba. J S Am Earth Sci 14: 307-317

Palandri JL, Kharaka YK (2004) A compilation of rate parameters of water-mineral interaction kinetics for application to geochemical modelling, U.S. Geological Survey, Open file report 2004-1068

Pelletier B (1996) Serpentines in nickel silicate ore from New Caledonia. Australasian Institute of Mining and Metallurgy Publication Series - Nickel conference, Kalgoorlie (Western Australia) 6/96 197–205

Power IM, Wilson SA, Dipple GM (2013) Serpentine carbonation for CO_2 sequestration. Elements 9: 115-121. doi: 10.2113/gselemnts.9.2.115

Proenza JA, Gervilla F, Melgarejo JC, Bodinier JL (1999) Al- and Cr-rich chromitites from the Mayarí–Baracoa Ophiolitic Belt (Eastern Cuba): consequence of interaction between volatile-rich melts and peridotite in suprasubduction mantle. Econ Geol 94: 547–566

Proenza JA, Tauler E, Melgarejo JC, Galí S, Labrador M, Marrero N, Pérez-Melo N, Rojas-Purón AL, Blanco-Moreno JA (2007) Mineralogy of oxide and hydrous silicate Ni-laterite profiles in Moa Bay area, northeast Cuba. In: Andrew et al. (eds.), Digging Deeper, Irish Association for Economic Geology, Dublin, Ireland. 2: 1389-1392

Quesnel B, Boulvais P, Gautier P, Cathelineau M, Cédric MJ, Dierick M, Agrinier P, Drouillet M (2016) Paired stable isotopes (O, C) and clumped isotope thermometry of magnesite and silica veins in the New Caledonia Peridotite Nappe. Geochim Cosmochim Acta 183: 234-249.

Rajapaksha AU, Vithanage M, Weerasooriya R, Dissanayake CB (2012) Surface complexation of nickel on iron and aluminum oxides: a comparative study with single and dual site clays. Colloid Surface A 405: 79-87

Richter A, Brendler V, Bernhard G (2005) Blind prediction of Cu(II) sorption onto goethite: Current capabilities of diffuse double layer model. Geochim et Cosmochim Acta 69: 2725-2734

Richter A, Brendler V (2008) Blind Prediction and Parameter Uncertainty – A Sorption Test Case. In M. Barnett O, Kent BD (eds) Developments in Earth and Environmental Sciences 7, Chapter 10

Rojas-Purón A, Simões Angélica R, Orozco-Melgar, O (2012) Identificación mineralógica de los óxidos de manganeso del yacimiento laterítico Punta Gorda, Moa, Cuba. Minería y Geología, 28: 1-26

Roqué-Rosell J, Mosselmans JFW, Proenza JA, Labrador M, Galí S, Atkinson KD, Quinn PD (2010) Sorption of Ni by "lithiophorite–asbolane" intermediates in Moa Bay lateritic deposits, eastern Cuba. Chem Geol 275: 9-18.

Rose AW, Bianchi-Mosquera GC (1993) Adsorption of Cu, Pb, Zn, Co, Ni and Ag on goethite and hematite. A control on metal mobilization from Red Beds into stratiform copper deposits. Econ Geol 88: 1226-1236

Singh B, Sherman DM, Gilkes RJ, Wells MA, Mosselmans JFW (2002) Incorporation of Cr, Mn and Ni into goethite (α-FeOOH): mechanism from extended X-ray absorption fine structure spectroscopy. Clay Miner 37: 639–649

~~Sokolova TA (2013) The destruction of quartz, amorphous silica minerals, and feldspars in model experiments and in soils: possible mechanisms, rates, and diagnostics (the analysis of literature). Eurasian Soil Sci+ 46: 91–105.~~

Soler JM (2013) Reactive transport modeling of concrete-clay interaction during 15 years at the Tournemire Underground Rock Laboratory. Eur J Mineral 25: 639–654

Soler JM, Cama J, Galí S, Melendez W, Ramirez A, Estanga J (2008) Composition and dissolution kinetics of garnierite from the Loma de Hierro Ni-laterite deposit, Venezuela. Chem Geol 249:191-202

Soler JM, Lasaga AC (1996) A mass transfer model of bauxite formation. Geochim Cosmochimi Acta 60: 4913-4931

Soler JM, Lasaga AC (1998) An advection-dispersion-reaction model of bauxite formation. J Hydrol 209: 311-330

Steefel CI (2009) CrunchFlow. Software for modeling multicomponent reactive flow and transport. User's manual. Lawrence Berkeley National Laboratory, Berkeley

Steefel CI and Lasaga AC (1994) A coupled model for transport of multiple chemical-species and kinetic precipitation dissolution reactions with application to reactive flow in single-phase hydrothermal systems. Am J Sc 294: 529–592

Steefel CI, Appelo CAJ, Arora B, Jacques D, Kallbacher T, Kolditz O, Lagneau V, Lichtner C, Mayer KU, Meeussen JCL, Molins S, Moulton D, Shao H, Simunek J, Spycher N, Yabusaki SB, Yeh GT (2015) Reactive transport codes for subsurface environmental simulation. Computat Geosci 19: 445–478. doi: 10.1007/s10596-014-9443-x

Strauss R, Brümmer GW and Barrow NJ (1997) Effects of crystallinity of goethite: I. Preparation and properties of goethites of differing crystallinity. Eur J Soil Sci 48: 87-99

Tauler E, Proenza JA, Galí S, Lewis JF, Labrador M, García-Romero E, Suárez M, Longo F, Bloise G (2009) Ni-sepiolite-falcondote in garnierite mineralization from the Falcondo Ni-laterite deposit, Dominican Republic. Clay Miner 44:435-454. DOI: 10.1180/claymin.2009.044.4.435

Thorne RL, Roberts S, Herrington R (2012) Climate change and the formation of nickel laterite deposits. Geology 40: 331-334

Trivedi P, Axe L (2001) Ni and Zn sorption to amorphous versus crystalline iron oxides: macroscopic studies. J Colloid Interf Sci 244: 221–229. doi:10.1006/jcis.2001.7970

Trivedi P, Axe L, Dyer J (2001) Adsorption of metal ions onto goethite: single-adsorbate and competitive systems. Colloid Surface A 191: 107–121

Ulrich M, Muñoz M, Guillot S, Cathelineau M, Picard C, Quesnel B, Boulvais P, Couteau C. (2014) Dissolution–precipitation processes governing the carbonation and silicification of the serpentinite sole of the New Caledonia ophiolite. Contrib Mineral Petr 167:952. doi: 10.1007/s00410-013-0952-8

Veneklaas EJ (1990) Nutrient fluxes in bulk precipitation and throughfall in two montane tropical rain forests, Colombia. J Ecol 78: 974-992

Villanova-de-Benavent C, Proenza JA, Galí S, García-Casco A, Tauler, E, Lewis JF, Longo F (2014) Garnierites and garnierites: Textures, mineralogy and geochemistry of garnierites in the Falcondo Ni-laterite deposit, Dominican Republic. Ore Geol Rev 58, 91–109

Villanova-de-Benavent C, Domènech C, Tauler C, Galí S, Tassara S, Proenza JA (2016a) Fe-Ni-Rich Serpentines from the Saprolite Horizon of Caribbean Ni-Laterite Deposits: a New insights from Thermodynamic Calculations. Miner Deposita. DOI 10.1007/s00126-016-0683-7.

Villanova-de-Benavent C, Nieto F, Viti C, Proenza JA, Galí S, Roqué-Rosell J (2016b) Ni-phyllosilicates (garnierites) from the Falcondo Ni-laterite deposit (Dominican Republic): Mineralogy, nanotextures, and formation mechanisms by HRTEM and AEM. Am Mineral 101, 1460–1473.

Wells MA, Ramanaidou ER, Verrall M, Tessarolo C (2009) Mineralogy and chemical chemistry of garnierites in the Goro lateritic nickel deposit, New Caledonia. Eur J Mineral 21:467–483.

Whitney DL Evans BW (2010) Abbreviations for names of rock-forming minerals. Am Mineral 95: 185-187.

Williams MR, Fisher TR, Melack JM (1997) Chemical composition and deposition of rain in the central amazon, Brazil. Atmos Environ 31: 207-217

Wolery TJ (1992) EQ3NR, a computer program for geochemical aqueous speciation-solubility calculations: Theoretical manual, user's guide and related documentation (Version 7.0). Publ UCRL-MA-110662 Pt III, Lawrence Livermore Lab, Livermore Calif.

Xu Y, Axe L, Boonfueng T, Tyson TA, Trivedi P, Pandya K (2007) Ni(II) complexation to amorphous hydrous ferric oxide:An X-ray absorption spectroscopy study. J Colloid Interf Sci 314: 10–17

Figure captions

Fig.1 Location and simplified geological map of the Moa Bay mining area (Cuba) showing the location of the Punta Gorda Ni-laterite deposit. Modified from Marchesi et al. (2006).

Fig. 2 Schematic representation of the studied profile of the Punta Gorda Ni-laterite deposit (a) and mineral composition of the analyzed samples (b). Mineral abbreviations taken from Whitney and Evans (2010) (Fo: forsterite, En: enstatite, Srp: serpentine, Mgh: maghemite, Gth: goethite, Hem: hematite, Gib: gibbsite, Qz: quartz), except pyrochroite (Prc). Modified from Galí et al. (2007).

Fig. 3 ~~Powder~~X-Ray diffraction diagram~~profile~~ of sample M4 from Punta Gorda. ~~In blue: the measured profile; in red: the total calculated profile; in purple: the calculated profile for goethite; in grey: the difference profile between observed and calculated profiles.~~ Agreement index Rwp = 10.31. Triangles at bottom are the position of the reflections used for calculating D_{hkl} values from measured 2θ and $FWHM_{hkl}$ values.

Fig. 4 Evolution of the amount of mineral (in wt.%) (areas) and of the amount of Ni sorbed onto goethite (in wt.% of Ni in goethite) (solid line) and porosity in the profile at initial time (0 y) and at different model elapsed times (from 10^3 to 10^6 years) for the Reference case.

Fig. 5. pH distribution at the profile at different time steps ~~Evolution of pH in the profile at different model elapsed times~~ for the Reference case.

Fig. 6 Distribution of Mg, Si, Fe and Ni aqueous concentration (a), goethite surface species (b), and pH (c) along the modeled profile after 1My of elapsed time.

Fig. 7 Amount of Mg, Si and Ni (in wt.%) leached out from the modelled profile after 10^6 years of elapsed time for the RC (R~~r~~eference case) and the different sensitivity ~~cases~~ analyses reported: *No_ads*, ~~case (~~without considering sorption of Ni onto goethite~~)~~, *Srp II** and *Srp II*$^\$$, ~~cases (~~considering different serpentine compositions, see Table ~~5~~4~~)~~, *Rate*, ~~case (~~considering faster dissolution rates of enstatie and forsterite~~)~~, *Less_carb*, ~~case (~~considering a smaller concentration of carbonate~~)~~ and *Qt*, ~~case (~~allowing quartz precipitation~~)~~.

Fig. 8 Distribution of the horizons along the modelled profile after 10^6 years of elapsed time for the RC (~~reference~~ Reference case) and the different sensitivity analyses ~~cases~~ reported (same abbreviations from ~~than in~~ Fig.7).

Fig. 9 Evolution of pH along the modelled profile after 10^6 years of elapsed time for the R~~r~~eference case and the different sensitivity analyses ~~cases~~ reported (same abbreviations from~~than in~~ Fig.7).

959

Table captions

~~**Table 1** Structural formulae of serpentine II, calculated on the basis of 7 oxygens from electron microprobe analyses (EMPA) of 8 individual samples.~~

Table ~~2~~ 1 pH, Eh (in V) and total concentration of components of rainwater and initial porewater (in mol/L). Mineral abbreviations ~~taken~~ from Whitney and Evans (2010)

Table ~~3~~2 Initial mineral composition considered in the model.

Table ~~4~~ 3 Solubility constants at 25ºC of the pure end-member phases used to calculate solubility constants of solid solutions used in the simulations. Mineral abbreviations ~~taken~~ from Whitney and Evans (2010).

Table ~~5~~ 4 Solubility constants at 25ºC calculated for the solid solutions used in the simulations. *$serpentines II used in the sensitivity cases. Mineral abbreviations ~~taken~~ from Whitney and Evans (2010).

Table ~~6~~ 5 Equilibrium constants for goethite surface reactions used in the calculations.

Table ~~7~~6 Summary of the main differences between the Reference ~~c~~case and the sensitivity analyses.~~cases of the modelling exercise.~~

Manuscript Without Track Changes
Click here to download Manuscript Without Track Changes manuscript_4threvision_changes_accepted.docx

Reactive transport model of the formation of oxide type Ni-laterite profiles (Punta Gorda, Moa Bay, Cuba)

Cristina Domènech[1], Salvador Galí[1], Cristina Villanova-de-Benavent[1], Josep M. Soler[2,3], Joaquín A. Proenza[1]

[1]Departament de Mineralogia, Petrologia i Geologia Aplicada, Facultat de Ciències de la Terra, Universitat de Barcelona (UB), C/ Martí i Franquès s/n - 08028 Barcelona, Catalonia, Spain

[2]Institute of Environmental Assessment and Water Research, IDAEA, CSIC, Jordi Girona 18-26, 08034, Barcelona, Catalonia, Spain

[3]Associated Unit: Hydrogeology Group (UPC-CSIC)

CORRESPONDING AUTHOR

Cristina Domènech – cristina.domenech@ub.edu. Telf +34 934 021 341. Fax + 34 934 021 340

ABSTRACT

Oxide type Ni-laterite deposits are characterized by a dominant limonite zone with goethite as the economically most important Ni ore mineral, and a thin zone of hydrous Mg silicate-rich saprolite beneath the magnesium discontinuity. Fe, less soluble, is mainly retained forming goethite, while Ni is redeposited at greater depth in a Fe(III) and Ni rich serpentine (serpentine II) or in goethite, where it adsorbs or substitutes for Fe in the mineral structure.

Here, a 1D reactive transport model, using Crunchflow, of Punta Gorda oxide type Ni-laterite deposit (Moa Bay, Cuba) formation is presented. The model reproduces the formation of the different laterite horizons in the profile from an initial, partially serpentinized peridotite, in 10^6 years, validating the conceptual model of the formation of this kind of deposits in which a narrow saprolite horizon rich in Ni-bearing serpentine is formed above peridotite parent rock and a thick limonite horizon is formed over saprolite. Results also confirm that sorption of Ni onto goethite can explain the weight percent of Ni found in the Moa goethite.

Sensitivity analyses accounting for the effect of key parameters (composition, dissolution rate, carbonate concentration, quartz precipitation) on the model results are also presented. It is found that aqueous carbonate concentration and quartz precipitation significantly affects the laterization process rate, while the effect of the composition of secondary serpentine or of mineral dissolution rates is minor. The results

of this reactive transport modeling have proven useful to validate the conceptual models derived from field observations.

KEYWORDS,

Oxide type Ni-laterites, Reactive Transport Modeling, Sorption, Goethite, Cuba

Introduction

Nickel laterite deposits are an important source of nickel and cobalt (Golightly 1981, 2010; Freyssinet et al. 2005, Lambiv Dzemua et al. 2013) and have potential for Sc and platinum group element by-products (Aiglsperger et al. 2016). Ni-laterite deposits formed from the chemical and mechanical weathering of ultramafic rocks exposed to the surface under favorable topography and climatic conditions. Laterite formation is controlled by intrinsic or extrinsic factors (Freyssinet et al. 2005, Moore et al. 2012, Butt and Cluzel 2013). Intrinsic factors include, among others, the chemical and mineralogical composition of protolith (mainly peridotite), the dissolution rate of minerals and the surface area. The geological context where laterite develop, the hydrological properties of the terrain (controlling water flow), the climate (temperature and rainfall) and the duration of the weathering process are examples of extrinsic factors that may condition laterite formation.

According to Golightly (1981, 2010) a typical Ni-laterite profile consists, from bottom to top of: a) partially or totally serpentinized ultramafic rock (protolith) characterized by unweathered minerals; b) saprolite horizon with textural features inherited from the protolith and dominated by secondary Si- and Mg- minerals; and c) limonitic horizon composed mainly of goethite that evolves to hematite with time. The interaction of slightly acidic meteoric water with the ultramafic bedrock causes the release of Mg, Si and Ni, which are transported downwards. In particular, Ni, less soluble, is redeposited at depth producing Ni-enriched zones. In the saprolite zone, Ni is mainly found in garnierite and/or secondary Ni-rich lizardite (serpentine II) and Ni-smectite (Pelletier 1996, Wells et al. 2009, Villanova-de-Benavent et al. 2014). In the limonitic horizon, Ni is mainly retained by goethite, either adsorbed or substituting Fe in the mineral structure, and by minor Mn- oxyhydroxides (Roqué-Rosell et al. 2010; Dublet et al. 2015).

Ni-laterites are usually classified according to their dominant Ni-bearing mineralogy in a) hydrous silicate type, b) clay type and c) oxide type (Brand et al. 1998; Freyssinet et al. 2005). Oxide type deposits, discussed in this contribution, are characterized by a dominant limonite horizon with goethite as the economically most important Ni ore mineral. These deposits represent about 60% of the current total Ni laterite resources, with mean grades ranging from 1.0 to 1.6 wt% Ni (Butt and Cluzel 2013).

Ni-laterites formed, or are currently forming (Butt and Cluzel 2013), under humid tropical climate, where rainfall is higher than 1000 mm/y and temperature ranges between 15-31 ºC (Freyssinet et al. 2005; Thorne et al. 2012). The mechanisms controlling the retention of Ni in goethite determine the mobility of

the metal and the supergene enrichment of the Ni-bearing phases in the laterite horizons (Roqué-Rosell et al. 2010; Dublet et al. 2012). However, the mechanisms controlling Ni mobility remain partly understood. The Ni-goethite association has been explained either by sorption of Ni onto the goethite surface (Cornell 1991; Rose and Bianchi-Mosquera 1993; Bryce et al. 1994; Coughlin and Stone 1995; Beukes et al. 2000; Trivedi and Axe 2001; Trivedi et al. 2001; Buerge-Weirich et al. 2002; Fisher et al. 2007; Arai 2008; Marcussen et al. 2009) or by the incorporation of Ni into the goethite structure or both (Manceau et al. 2000; Singh et al. 2002; Carvalho-e-Silva et al. 2002, 2003; Fan and Gerson 2011; Dublet et al. 2012). Sorption of Ni on goethite has been studied both in natural and synthetic goethite by means of sorption experiments and spectroscopic techniques. Ni sorbs onto goethite forming inner-sphere mononuclear bidentate complexes (Trivedi et al. 2001; Xu et al. 2007), and sorption increases from pH 5 to 8 (Rose and Bianchi-Mosquera 1993; Beukes et al. 2000; Buerge-Weirich et al. 2002; Arai 2008). Sorption of Ni onto goethite has been modelled by considering Langmuir isotherms (Trivedi et al. 2001), a Diffuse Layer Model (Bryce et al. 1994; Buerge-Weirich et al. 2002; Marcussen et al. 2009; Rajapaksha et al. 2012) or a Triple Layer Model (Coughlin and Stone 1995).

The incorporation of Ni in the goethite structure is facilitated by the similar ionic radii between Fe^{3+} (0.64Å) and Ni^{2+} (0.69Å). However, even this small difference changes cell parameters, and together with the difference in charge between both cations, limits the maximum amount of Ni in goethite (Dublet et al. 2015). According to Cornell (1991), 15% of sites occupied by Fe in goethite can be substituted by other cations without destabilizing the goethite structure. Manceau et al. (2000) studied natural goethite by extended X-Ray Absorption Fine Structure (EXAFS) and showed that Ni was partially incorporated in the goethite structure. Singh et al. (2002) demonstrated up to 5 mol % isomorphic substitution of Ni^{2+} in the FeOOH structure which was limited by changes in the next-nearest-neighbour coordination environment. Differential thermal (DTA), thermal gravimetric (TGA) and EXAFS analyses of natural lateritic goethite (1.8-4.1 mol% Ni) by Carvalho-e-Silva et al. (2002, 2003) suggested that the charge imbalance could be compensated by the incorporation of H^+ into the goethite structure. Fan and Gerson (2011) indicated that Ni associated with goethite in Philippine laterite was substituting Fe within its structure. Dublet et al. (2012) and Cathelineau et al. (2016) studied the speciation of Ni in a New Caledonian laterite profile and observed Ni-goethite as the predominant Ni-bearer.

Bryce et al. (1994) considered that although sorption should be reversible, because of aging or hysteresis Ni might not be completely released from goethite surface. Dublet et al. (2015) stated that the

incorporation of Ni in goethite may be affected by the sequence of dissolution-precipitation reactions forming goethite. Therefore, in spite of evidence of both sorption of Ni on the goethite surface and its incorporation in the structure, there is still a lack of understanding of these processes.

In order to test the validity of conceptual models derived from field and/or experimental observations, reactive transport and geochemical modeling has proven successful (Soler and Lasaga 1998; Corbella et al. 2004). There are several computer codes available to perform reactive transport or geochemical calculations (Steefel et al. 2015), although none of them can consider all hydro-geochemical processes simultaneously.

Soler and Lasaga (1996, 1998) developed one dimensional models of bauxite (Al-laterite) formation, describing the alteration of a granitic protolith and the formation of the bauxite and saprolite horizons over long time scales (10^6 years) using mineral reaction kinetics. Fletcher et al. (2006) performed a simple two-mineral model to study how weathering can transform intact bedrock into saprolite. The model coupled physical processes (e.g. fracturing) to chemical processes (e.g. mineral dissolution) and the rate of displacement of the reaction front was shown to depend on the composition of the reactant fluid where O_2 and CO_2 are the most critical components in the case of a Puerto Rico quartz diorite regolith. Lebedeva et al. (2007) incorporated saprolite-forming reactions and developed a four-mineral model to predict rates of formation of saprolite, whereas Fletcher and Brantley (2010) developed a simplified one dimensional model to study a weathering profile, including vertical fluid transport, kinetic reaction and erosion.

Navarre-Sitchler et al. (2011) used the reactive coupled transport code CrunchFlow to simulate the chemical and physical transformations during weathering of a basaltic rock and compared their results with field observations of alluvial terraces in Costa Rica, where erosion was not significant. They used a 1D model of a total length of 100 mm and observed that for porosities higher than 9%, mineral reaction kinetics dominated over transport, and that the advance of the weathering front was controlled by the rate at which porosity was created.

Moore et al. (2012) modeled the dissolution of minerals in a granitic soil and in a granitic saprolite with the reactive transport model FLOTRAN. The modeled reaction front depth was highly dependent on the precipitation rate of secondary minerals and on fluid flow. Moreover, they had to use reduced reaction rates, compared with rates from laboratory studies, to fit the field observations. They concluded that

reactive transport models can be used to understand the long-lived (10^6 years) mineral weathering processes given that they consider the simultaneous non-linear processes.

In this study, a reactive transport model is used to simulate the formation of the oxide type Punta Gorda Ni-laterite deposit from an initial partially serpentinized peridotite at constant temperature (25ºC). The Punta Gorda deposit is part of the Moa Bay mining area, one of the largest reserves of nickel and cobalt in the world (Linchenat and Shirakova 1964; Lavaut 1998; Lewis et al. 2006; Proenza et al. 2007; Aiglsperger et al. 2016), and probably the best known example of Ni-laterite deposits of oxide type (Gleeson et al. 2003).

The main objective of this contribution is to test a conceptual model for the formation of oxide type Ni-laterite deposits and to identify and quantify, the key parameters affecting the development of the different laterite horizons. Moreover, by considering that Ni is sorbed onto goethite, we aim to determine whether this process could account for the amount of Ni found in the goethite at Punta Gorda.

In this paper, we present a modeling exercise that provides valuable insights into the understanding of the formation of Ni-laterite deposits. The modeling consists of a set of one dimensional models in which rain water infiltrates and flows vertically downwards simulating the infiltration through fractures and cracks. Formation of the goethite and saprolite horizons is achieved by dissolution of primary minerals and precipitation of secondary minerals. No solid solutions have been included for simplicity. Porosity changes reflecting different molar volumes of dissolving/precipitating minerals are taken into account. Due to fact that the model is one dimensional, it does not account for the formation of typical saprolite corestones as lateral water flow and matrix diffusion processes are not considered. Water is allowed to equilibrate with air along the whole domain, simulating unsaturated conditions. Calculations have been carried out for a time span of 10^6 years. Past climatic changes, such as variations in precipitation regime, erosion, or collapse due to increase in porosity in the upper part of laterite profile are not considered.

The 1D models described here differ in values for several parameters that preliminary work had identified as having a significant role in the formation of laterite profiles, such as solubility constants, dissolution rates, CO_2(g), precipitation of quartz. A Reference case model is explained in detail whereas the results of the other models are compared to the results of the Reference case.

The Punta Gorda Ni-laterite deposit

The Punta Gorda Ni-Co laterite deposit is located in the Moa Bay mining area (northeast of Cuba; Fig.1). The Moa Bay laterite deposits are part of a larger province of nickel laterite in northeast Cuba. The deposits developed over serpentinized harzburgite of Moa-Baracoa ophiolitic massif (Proenza et al. 1999; Marchesi et al. 2006) with weathering and laterization commencing during the Miocene (Lewis et al. 2006; Proenza et al. 2007). The elevation of the peneplain surface of the deposits varies from 60 to 950 m above sea level, and the weathering mantle can reach a total thickness of more than 50 m in the laterite profile (Linchenat and Shirakova 1964; Golightly et al., 2008b).

This deposit can be classified as oxide type (Oliveira et al. 2001; Rojas-Purón et al. 2012; Aiglsperger et al. 2016). As with many northeastern Cuban deposits, the typical vertical section consists of four principal horizons, from bottom to top: (1) parent rock serpentinized peridotite, (2) saprolite, (3) lower and upper limonite and (4) ferricrete or duricrust (Lewis et al. 2006; Proenza et al. 2007; Aiglsperger et al. 2016; Fig. 2a). Occasionally, within a profile some gabbro bodies weather to bauxite. Ni and Co are mainly in the limonite zone but the siting of metals (adsorbed or in solid solution) remains debated.

The Punta Gorda deposit has been extensively studied (Oliveira et al. 2001; Galí et al. 2007; Roqué-Rosell et al. 2010; Rojas-Purón et al. 2012; Aiglsperger et al. 2016). The mineralogy was characterized by qualitative and quantitative X-Ray diffraction, optical and scanning electron microscopy (SEM) and electron probe microanalysis (EPMA; Galí et al. 2007). Concentrations of major and minor elements as well as trace elements in parent rocks and weathering products of Ni-laterite profiles were measured by Aiglsperger et al. (2016).

The mineralogical composition of the studied profile in Punta Gorda is shown in Fig. 2b. The main minerals of the parent serpentinized peridotite are forsterite, enstatite, serpentine and maghemite (Sample M10). The saprolite horizon is dominated by serpentine and goethite (Sample M9), whereas in limonite and ferricrete horizons, goethite and hematite are the main minerals, although other minor phases such as pyrochroite, gibbsite, quartz, Mn-oxyhydroxide aggregate (lithiophorite, “lithiophorite–asbolane intermediates”) and asbolane (Roqué-Rosell et al. 2010) are also found (samples M8 to M1).

The parent rock from which the Ni-laterite profile in the Moa district originated consists of partially serpentinized ophiolitic harzburgite (70% $Mg_9Fe_{0.95}Ni_{0.05}Si_5O_{20}$, 16% $Mg_9FeSi_{10}O_{30}$) including plagioclase-rich bodies, which was exposed to the surface during the late Miocene ($\approx 10^7$ years; Lewis et al. 2006). Serpentine minerals are politype 1T and 2H1 lizardite. Lizardite 1T is the dominant politype whereas lizardite 2H1 is less crystalline and presents many stacking faults in its structure. The cell

volume is slightly larger than that corresponding to the ideal end member $Mg_3Si_2O_5(OH)_4$, due to substitution of Mg by Fe and minor Ni and Mn, as confirmed by chemical analyses. Two different types of serpentine have been identified. Serpentine I formed by alteration of forsterite and enstatite during a hydrothermal stage, whereas serpentine II formed after weathering of serpentine I. Serpentine II can be formed as a thermodynamically stable secondary phase in meteoric conditions, as shown in Villanova-de-Benavent et al. (2016a). Serpentine I composition, calculated from EPMA data is $Mg_{2.85}Fe_{0.14}Ni_{0.01}Si_2O_5(OH)_4$. In serpentine II, Mg in octahedral coordination is partially substituted by Fe^{3+} and Ni^{2+}. Serpentine II structural formulae calculated from EPMA are shown in Online resource 1. Serpentine II contains more Ni than serpentine I. The Ni-bearing serpentine (Srp-II), in addition to "garnierite", is the main Ni ore in saprolite horizon of Ni-laterite deposits (Golightly and Arancibia 1979; Pelletier 1996; Villanova-de-Benavent et al. 2014, 2016b). In the case of Punta Gorda deposit, this second generation of serpentine is the major Ni-bearing silicate phase in the saprolite horizon. Nickel content in Ni-rich serpentine ranges from 1 to 7 wt.% NiO, in contrast with serpentine I, which has the same Ni content than the olivine (~ 0.4 wt.%).

Iron oxides are maghemite, goethite and hematite. The refined cell parameter of maghemite, very similar to the accepted value of 8.3505 Å, indicates a composition near the ideal Fe_2O_3 (Galí et al. 2007). In near surface conditions, maghemite can form by oxidation of magnetite (Gehring et al. 2009, Lilova et al. 2012) that in turn, results from the hydration of primary olivine and pyroxene. Under atmospheric conditions, maghemite is transformed into goethite. Hematite (Fe_2O_3) has almost an ideal composition and structure, although it has a low crystallite size (30 to 40 nm; Galí et al 2007). Goethite (FeOOH), the major phase containing most of the Ni in this profile (from 0.8 to 4 wt.% with an average value of 1.23 wt.%), coexists with maghemite and hematite in limonite samples and with lizardite in samples M8 and M9 (Galí et al. 2007). Crystallographic studies indicate that there is some substitution (2-17%) of Fe by Al as the cell volume is always smaller than the accepted value for goethite. The analysis of different diffraction peaks of goethite using the Scherrer's relation (Klug and Alexander 1962; Langford 1978; De Keijser et al. 1982; Louër et al. 1983) and using values for the 110, 020, 120 and 130 peaks in the space group P_{bnm} (a=4.605 Å, b=9.96 Å and c=3.02 Å; Fig. 3), and a value of $\lambda[K\alpha1,Cu]$ of 1.5406 Å, yields an ideal mean elongated prism in the **c** direction, with 8.7 nm in the **a** direction and 18.1 nm in **b** direction**.** The length in **c** could not be determined, but observations have shown that the c/b aspect ratio is not less than 4.5 (Strauss et al. 1997). With these data, the calculated specific surface for goethite is 84.8 m^2/g. If,

instead of adjusting a prismatic shape, an elliptical cylinder elongated in the **c** direction is fitted, a specific surface of 87.2 m^2/g is obtained, which is similar to the previous value.

The specific surface obtained by the BET (Brunauer-Emmet-Teller) method (Brunauer et al. 1938) for the same material is 65.2 m^2/g. As expected, the BET value is lower than the value calculated through X-Ray diffraction which reflects the dimension of the coherent diffracting domains, rather than the dimension of the material particle that consists of an aggregate of several domains.

Materials and methods

The reactive transport model presented in this work is based on the direct formation conceptual model described in Butt and Cluzel (2013). According to this model, oxide type Ni-laterite deposits form as a result of continuous weathering of partially serpentinized peridotite under tropical climate. During weathering, the water table is high and fluctuating, and erosion rates are low. The system is fully saturated. Meteoric water, in equilibrium with atmospheric O_2 and CO_2, flows through the profile at a constant rate. Therefore, Ni is expected to be released from olivine or serpentine I and retained by the formation of a Fe(III)-rich serpentine II and by sorption onto goethite, while Mg and Si are expected to be leached out of the system (Ulrich et al. 2014, Villanova-de-Benavent et al. 2016a) because of serpentine and silicate dissolution. Dissolution can cause an increase in porosity that may accelerate the processes due to the decreased solid/water ratio.

According to Butt and Cluzel (2013), Ni may be leached from goethite to garnierite deeper in the profile, and goethite may transform to hematite, particularly in the upper most limonite horizon. Neither the formation of garnierite, nor the formation of hematite, is considered in this model.

Temperature is considered constant at 25 ºC. According to Thorne et al. (2012), Ni-laterite forms in tropical areas where monthly temperatures are in the range of 22-31 ºC in the summer and between 15-27 ºC in the winter.

The partially serpentinized unweathered peridotite is composed of Ni-bearing forsterite, enstatite and serpentine I. In our model, maghemite is not considered given its low stability. Its precursor, magnetite is considered instead (Gehring et al. 2009). Serpentine I and magnetite formed during a previous hydrothermal serpentinization event (pre-weathering), that is outside the scope of this study.

Chemistry solver, modeled domain and hydrodynamic system

The computer code used for the simulations is Crunchflow, a software package for simulating reactive transport developed by Steefel and co-workers (Stefeel and Lasaga 1994; Stefeel 2009). This code can take into account aqueous speciation, surface complexation, ion exchange, mineral dissolution/precipitation and transport processes under fully saturated flow conditions and variable temperature (Steefel et al. 2015). All mineral transformations are treated as dissolution and precipitation reactions. Kinetic reaction rates, depending on reactive surface area, are used to describe these reactions. Transformations in the solid state (without dissolution/precipitation) are not considered. However, if reaction rates are fast compared to solute transport by advection, dispersion or diffusion, when the dissolution of a mineral can cause supersaturation of the solution with respect to another phase, this new phase will precipitate at the same location as that of the dissolving mineral, causing an effect similar to a potential solid-state transformation. The code uses an integrated finite difference discretization to solve the advection-dispersion-reaction differential equations that link flow, solute transport and geochemical processes. Total porosity (ϕ_T) is updated after each time step according to eq. 1, where N_m is the number of minerals in the model (Navarre-Sitchler et al. 2011) and ϕ_m, the volume fractions of minerals.

$$\phi_{\mathrm{T}}=1-\sum_{k\text{-}1}^{N_m}\phi_m \qquad (1)$$

The ϕ_m values are updated after each time step according to eq. 2, where *t-1* indicates the parameter value of the previous time-step, Δt is the time step length (s), V_m the molar volume of the mineral (m^3/mol) and R_m the mineral reaction rate (mol/m^3/s). Rate equations follow the Transition State Theory (Lasaga 1998) and are calculated according to eq. 3 where A_m is the mineral surface area (m^2/m^3_{rock}), k_{25}, the reaction rate constant (mol/m^2/s) at 25ºC, R is the gas constant (8.3144 J/mol/K), E_a is the activation energy (J/mol), T is temperature (K), a_i^{ni} is the term describing the effect of species i on the rate, and $\mathrm{f_m}(\Delta\mathrm{G})$ is the function describing the dependence of the rate on the solution saturation state (Soler 2013). This function is calculated with eq. 4 where IAP is the ionic activity product of the solution with respect to the mineral, K_{eq} is the equilibrium constant of that mineral, and m_1, m_2 and m_3 are empirical parameters defining the shape of this function (assumed to be equal to 1 if no experimental data are available).

$$\phi_m=\phi_{m,t\text{-}1}+V_m(R_m\Delta\mathrm{t}) \qquad (2)$$

$$R_m=A_m\sum_{\mathrm{terms}}k_{25}e^{\frac{-\mathrm{E_a}}{R}\left(\frac{1}{T_{25}}-\frac{1}{T}\right)}\left(\prod_{\mathrm{i}}a_i^{n_i}\right)\mathrm{f_m}(\Delta\mathrm{G}) \qquad (3)$$

$$\mathrm{f_m}(\Delta\mathrm{G})=\left[1\text{-}e^{\left(m_2\left(\ln\frac{\mathrm{IAP}}{K_{eq}}\right)^{m_3}\right)}\right]^{m_1} \qquad (4)$$

The mineral surface area (A_m) is calculated according to eq. 5 where, $A_{specific}$ is the mineral specific surface area (m^2/g) and MW_m, the mineral molecular weight (g/mol). A threshold mineral volume fraction value must be provided for secondary minerals not initially present in the system to calculate the bulk surface area until the computed time-evolving volume fraction exceeds the threshold value.

$$A_m = \frac{\emptyset_m A_{specific} \mathrm{MW_m}}{V_m} \quad (5)$$

Activity coefficients for aqueous species are calculated according to the extended Debye-Hückel equation (Steefel 2009).

The physical system chosen to conduct the reactive transport model is a 1D column of 88 m length representing the laterite profile. In the model, rainwater flows from top to bottom. The column is discretized into a mesh of 250 elements of 0.35 m length each. Models are run for 10^6 years, with a maximum time step of 1 year. Meteoric water has a constant composition (Table 1), typical of rainwater from tropical areas (Veneklaas 1990; Williams et al. 1997; Bertolo et al. 2006). It has an ionic strength of 1.4×10^{-4} mol/L. pH has been set to 4.5, accounting for both the acidic pH of rainwater and the acidity generated in soils due to the formation of organic acids as a consequence of organic matter decomposition (Soler and Lasaga, 1996). Rainwater is flowing along the column at a constant rate during modeling. The average annual rainfall at Moa in the period 1900-2009 is 1360 mm, of which 990 mm fall during the two wet seasons (data from http://sdwebx.worldbank.org/climateportal). This value agrees with the values between 900 and 1800 mm/y reported by Butt and Cluzel (2013) as summer rainfall for laterite deposit in Caribbean areas. Assuming retention by the soil of 15% (Veneklaas, 1990) the infiltration flow rate is 1156 mm/y (4.0×10^{-8} $m^3/m^2/s$).

Neither dry periods nor changes in the infiltration rate are considered during the modeling. Transport is mainly advective. A water diffusion coefficient for solutes of 1.0×10^{-10} m^{-2} s^{-1} is used and dispersivity is assumed to be equal to 1 m based on the length of the domain (88 m). Diffusive and dispersive transport is not significant.

Geochemical system

Initially, the system has a homogeneous mineralogical composition, representing the partially serpentinized peridotite (Table 2). Initial mineral volume fractions are based on field observations in the Punta Gorda laterite deposit (M10 sample in Fig. 2b). An initial porosity of 12 % is used to account for

the fracture porosity. En_{90} and Fo_{90} are chosen as representative of the pyroxene and olivine from the unaltered peridotite, respectively.

Initial porewater composition is calculated to be in equilibriun with this set of minerals (Table 1). It has an ionic strength of 1.1×10^{-4} mol/L. K and Na are found as free ions, Si is forming aqueous H_4SiO_4 (68%) and $H_3SiO_4^-$ (32%). The most abundant aqueous species of carbonate at pH 9.5 is HCO_3^- (86%) although CO_3^{2-} is also significant (13%), together with minor amounts of $MgCO_3$(aq) and $FeCO_3$(aq) (<1%). All iron is found as Fe(II), and is present as Fe^{2+} (50%), $FeOH^+$ (48%) and $Fe(OH)_2$(aq) (2%). Mg aqueous speciation is dominated by Mg^{2+} (99%) although a small amount of $MgOH^+$ (1%) is computed. Finally, the main Ni aqueous species are $Ni(OH)_2$ (83%), Ni^{2+} (9%) and $NiOH^+$ (8%).

Besides the primary minerals considered in the initial composition, serpentine II and goethite are included in the calculations and are allowed to precipitate in the case where porewater is saturated with respect to those minerals. Although several compositions for serpentine II are available (Online resource 1), only one composition was used in the model for sake of simplicity. In the Reference case, the composition is set to $Mg_{2.798}Fe_{0.102}Ni_{0.049}Si_2O_5(OH)_4$ but the effect of different compositions has been studied in sensitivity analyses.

In many oxide deposits abundant secondary silica has been observed in the form of chalcedony or quartz (Butt and Cluzel 2013). In the model presented here, the saturation index of quartz is monitored and the formation of quartz is considered in a sensitivity analysis.

Moore et al. (2012) highlighted the role of weathering of silicate mineral as a sink for atmospheric CO_2(g). Magnesite deposits associated to serpentine bodies have been reported (Foster and Eggleton 2002; Ulrich et al. 2014; Quesnel et al. 2016). However, magnesite precipitation, although thermodynamically stable, is inhibited in near surface environments given the strong hydration shells that form around Mg^{2+} ions (Power et al. 2013; Morgan et al. 2015). In these conditions, Königsberger et al. (1999) suggested that hydrated magnesium carbonate minerals, such as nesquehonite ($MgCO_3\cdot3H_2O$) form instead. Power et al. (2013) reported that CO_2(g), in turn, may affect the weathering rate of silicate mineral. In order to elucidate the effect of CO_2 in the formation of this type of deposits, the saturation index of nesquehonite is monitored and the effect of different CO_2(g) concentrations is considered in sensitivity analysis.

Thermodynamic and kinetic data

Thermodynamic data used in the calculations for aqueous species and for the dissolution/precipitation of quartz and goethite are from ThermoChimie v.9 database (Giffaut et al. 2014). The total list of solute species included in the simulations is shown in Online resource 2.

Solubility constants for En_{90}, Fo_{90}, serpentine I and serpentine II have been modified given that they are not pure magnesium end member minerals. An ideal solid solution between pure end members has been considered for each mineral. For an ideal solid solution $A_{\chi}B_{(1-\chi)}C$, where the pure end members are AC and BC, the solubility constant of a given discrete composition can be calculated using eq. 6, where K_{AC} is the solubility constant of pure AC, K_{BC} is the solubility constant of pure BC and χ the molar fraction of A in the solid solution.

$$K=(K_{AC}\chi)^{\chi}\left(K_{BC}\left(1-\chi\right)\right)^{1-\chi} \quad (6)$$

The pure end members considered for Fo_{90} are fayalite (Fe_2SiO_4), forsterite (Mg_2SiO_4) and the phase Ni_2SiO_4; for En_{90}, the pure end members are enstatite ($MgSiO_3$) and ferrosilite ($FeSiO_3$). In the case of serpentine I the pure end members are lizardite ($Mg_3Si_2O_5(OH)_4$), népouite ($Ni_3Si_2O_5(OH)_4$) and greenalite ($Fe_3Si_2O_5(OH)_4$) while in the case of serpentine II, Fe(III)-lizardite ($Fe_2Si_2O_5(OH)_4$) is considered instead of greenalite to account for the difference of the valence state of Fe in the octahedral site. The log K values of these pure end members are taken from ThermoChimie v.9 when available. Additional log K values (e.g. forsterite) are calculated from ΔG_r^o or ΔG_f values from literature (Villanova-de-Benavent et al. 2016a). Selected log K values for pure end-members are listed in Table 3, whereas log K values calculated for the solid solutions are in Table 4.

In CrunchFlow, dissolution/precipitation of minerals is kinetically controlled. As dissolution and/or precipitation of serpentine I, serpentine II, goethite and magnetite is considered to occur under local equilibrium, the rates for these minerals have been modified in order to rapidly achieve equilibrium (large surface areas and/or large rate constants). The threshold volume fraction considered is 10^{-8} and10^{-4} for goethite and serpentine II, respectively.

Dissolution rates for Fo_{90} and En_{90} are assumed equal to those for pure forsterite and enstatite reported in Palandri and Kharaka (2004). The assignment of a value for the reactive area of forsterite and enstatite is not straightforward. Dissolution rates measured in the laboratory are 2 to 5 orders of magnitude faster than in field due to a variety of factors such as the presence/absence of inhibitors or catalyzers such as organic acids, hydrologic regimes, armoring of natural surfaces or the affinity of secondary minerals (Navarre-Sitchler et al. 2011). After preliminary calculations, a reactive area of 0.0005 m^2/g for Fo_{90} and

of 0.005 m^2/g for En_{90} is considered in the model. These values give results comparable to field observations. Nevertheless, the effect of higher surface areas is studied in sensitivity analyses. Mn-oxyhydroxides have not been considered.

The Ni content in the goethite from Punta Gorda ranges from 0.8 to 4.0 wt.% Ni. In the model presented here, this Ni is sorbed onto the goethite surface. Assuming that when the Ni content is 4.0 wt.% all surface sites are occupied by Ni, the maximum sorption capacity of goethite can be calculated, being 6.5 sites/nm^2 for a surface area of 65.2 m^2/g. This value is consistent with the values proposed by Davis and Kent (1990) (2.6-16.8 sites/nm^2 for Fe oxyhydroxides), or Hayes and Leckie (3-11 sites/nm^2). Information concerning the sorption of Ni onto goethite is scarce (Marcussen et al. 2009; Rajapaksha et al. 2012). Sorption of Ni onto the goethite surface is modeled following a one-site non electrostatic sorption model based on Marcussen et al. (2009) (Table 5), where Ni sorbs onto goethite surface forming the surface complex >Fe_ONi$^+$. These authors used a log K for goethite surface protonation/deprotonation from Richter et al. (2005) but an update of these values (Richter and Brendler 2008) is used in our study. The original log K values were provided for a density site of 2.31 sites/nm^2 and they have been recalculated to account for the site density of Punta Gorda goethite according to eq. 7 (Richter et al. 2005), where K are the sorption equilibrium constants, Γ the site density (sites/nm^2), and the subscript *o* stands for the new values calculated for 6.5 sites/nm^2. Total sorption capacity of goethite is 0.0625 moles sites/moles goethite.

$$\log K_o = \log K + \frac{\Gamma}{\Gamma_o} \qquad (7)$$

Results and discussion

The modeling results presented in this paper consists of a Reference case whose initial and boundary conditions have been detailed above and a set of Sensitivity analyses in which some parameters have been modified with respect to those of the Reference case.

Reference case

The residence time of water in the profile is 2.7 years. This residence time is very short compared to the total time of modeling (10^6 years) and indicates, as expected, that the influence of the initial porewater composition on the final results can be neglected.

Fig. 4 shows the evolution of the mineral composition (% wt), sorbed Ni concentration, and porosity as a function of depth at different elapsed times. When looking at Fig. 4 the reader must take into consideration that the weight percentage of a given mineral can increase either because of its precipitation or because of the dissolution of other minerals without precipitation. In order to simulate the effect of unsaturated flow, once the model run starts, porewater is equilibrated with atmospheric O_2(g) and CO_2(g) all along the profile. Due to O_2(g) equilibrium, magnetite becomes unstable and is transformed into goethite, serpentine II precipitates, and porosity decreases before 1000 years of elapsed time to values down to 5% (Fig. 4). Although this is realistic, changes at the bottom of the weathering profile are an artifact caused by the assumption of equilibrium with atmospheric O_2(g) and CO_2(g). Given the impossibility of fixing a realistic depth in which the system changes from unsaturated to saturated conditions, we have carried out the *Less_carb* sensitivity case in which only the infiltrating rainwater (not along the profile) is in equilibrium with atmospheric O_2(g) and CO_2(g).

During the first 1000 years, two different reactions are observed to occur in the profile. Dissolution of En and Fo occurs all along the profile, while precipitation of Srp I and Srp II occurs along the profile, except at the top. pH is buffered to 8.6 (Fig. 5) and Ni aqueous concentration is low ($<10^{-15}$ mol/L). The main species occupying the goethite surface is >FeOH (>95%).

However, at the top of the profile, where rainwater is acidifying the system, Srp I dissolves together with Fo_{90} and En_{90} and the saprolite horizon begins to develop. Srp II and goethite precipitate removing Ni and Fe from solution. In fact, the amount of Srp II precipitating depends on the amount of Ni released from the dissolution of Fo_{90} and Srp I. Fe released by En_{90}, Fo_{90} and Srp I that has not been incorporated into Srp II, precipitates as goethite. The presence of both Srp I and Srp II buffers pH at a value of 8.6 and causesNi aqueous concentration remain at very low values. Goethite surface speciation is dominated by >FeOH.

Between 1000 and 10000 years of elapsed time, no significant changes are observed, except that, at the top of the profile, Srp I has been exhausted. As a consequence, porosity has significantly increased. However, as Fo_{90} and En_{90} are still in the system, they dissolve and Srp II and goethite precipitate. Although in the model Fo_{90} is the first silicate mineral to dissolve followed by En_{90}, as observed by Freyssinet et al. (2005), Golightly (2010) and Hewawasam et al. (2013), their coexistence with Srp II and Gth without Srp I is not in agreement with the paragenesis observed in the field in which neither enstatite nor forsterite are in contact with Srp II. One of the most uncertain parameters in reaction kinetics is the

choice of reactive area, which suggests that the reactive areas used in the Reference case could be too low. In any case, this is a transitory effect that is not observed after 10^6 years of elapsed time.

Between 1000 and 10000 years of elapsed time, a new horizon starts to develop in the model first node, in contact with the infiltrating rainwater. The precipitation of goethite has increased its sorption capacity and causes the dissolution of Srp II because Ni is preferentially sorbed onto the goethite surface (>FeONi$^+$). pH decreases from 8.6 to a buffered value of 8.3. Ni aqueous concentration is close to 10^{-8} mol/L.

During the period 10^4 – 10^5 years, two significant observations can be made. On one hand, Fo_{90} is exhausted, which means that the only processes controlling Ni concentration in solution are the formation of Srp II and the sorption of Ni onto goethite surface. On the other hand, a new oxide horizon is starting to form at the top of the profile because Srp II has been dissolved. pH is no longer buffered at 8.3. Enstatite is dissolving yielding Fe that precipitates as goethite. As a consequence, the porosity increases up to 75%. The formation of >FeONi$^+$ displaces H^+ from the goethite surface (Table 5) and contributes to the decrease of pH together with the input of acidic water. Ni aqueous concentration is about 3×10^{-7} mol/L.

At 10^5 years of elapsed time, the three main horizons of a typical laterite profile have formed (Fig. 4). At the top of the column, there is the goethite-dominated horizon; below 10 m depth, Srp I is in equilibrium with Srp II and Gth at pH 8.6 in a partially weathered peridotite horizon, and between both layers, there is a narrow horizon in which serpentine II is in equilibrium with a goethite with Ni sorbed, the saprolite horizon (Fig. 4).

From 10^5 years on, slight changes are predicted. The oxide and saprolite horizons develop and the interfaces are displaced towards greater depths. At the top of the profile, there is no more forsterite providing Ni to the system and the pH is acid, such that desorption of Ni increases Ni aqueous concentration. At 4×10^5 years of elapsed time, enstatite is exhausted and goethite becomes the only phase in this horizon. pH is 4.5 and porosity is high, about 91% (Fig. 4). Ni released from the goethite surface is sorbed downflow on the goethite in the saprolite horizon until its surface is saturated (at 8×10^5 years of elapsed time). From this moment, saprolite horizon develops faster given that no more Ni can sorb onto goethite and it is available for serpentine precipitation.

The model results obtained agree with the laterite formation rates reported in literature. In 10^6 y, the thickness of weathered laterite might be 10-20 m (Freyssinet et al. 2005), 29-58 m (Golightly 2010) or 2-75 m (Hewawasam et al. 2013). Hewawasam et al. (2013) observed that in Sri Lanka laterites, weathering

processes are occurring at the reaction front, and are displaced towards greater depths as minerals become weathered. According to Goodfellow et al. (2011) this is because weathering reactions are inhibited in those areas where porewater is saturated with respect to weathering products that is, far from the water table, and in contrast, weathering is enhanced in the vadose zone. In agreement with those authors, in the model presented here, the reaction front starts at the top of the profile and is moving downward with time as weathering reactions progress.

The model satisfactorily explains the formation of the three different horizons observed in the field in a period of time around 10^6 y. The first one, with a thickness of 61 m, is at the top of the profile and is composed of goethite. In this horizon, the porosity is high (Fig. 4), porewater composition is poor in Mg, Si, Fe and Ni, pH is around 4.5 and the goethite surface is saturated with H^+ (Fig. 6).

The second horizon is formed by goethite and serpentine II. It has a thickness of 11 m with an average porosity of 40%, although it increases at the bottom. pH increases up to 8.3 and goethite contains up to 4 wt.% Ni sorbed onto its surface. The main surface species is >Fe_ONi$^+$. (Fig. 6). In this saprolite horizon, the ratios between Mg/Si and CO_3/Mg in solution are 1.4 and 2.0 respectively, in agreement with the observations of Golightly (1981). pH values also agree with those reported for saprolite horizons (Golightly 1981, 2010; Pelletier 1996).

Another similitude with field observations is the difference between the development of the limonitic and saprolite horizons. The larger thickness of the limonitic horizon in relation to that of saprolite has been observed in areas with maximum lixiviation (Butt and Cluzel 2013), and unsaturated conditions, i.e. porewater in equilibrium with atmospheric O_2(g) and CO_2(g). Nevertheless, the goethite horizon is significantly thicker (61 m) than the saprolite horizon (11 m), due to the fact that the model does not take into account the collapse of this horizon. In case of collapsing, the thickness of the goethite horizon will be smaller and similar to that observed in the Punta Gorda deposit (30m, Fig. 1).

The third and deepest horizon, with a depth limited by model dimensions, represents a partially weathered serpentinized peridotite, with serpentine I in equilibrium with serpentine II and goethite. pH is 8.6 and Ni is not sorbed onto goethite (Fig. 6). Porosity is low, close to 5%.

After 10^6 y, 76% of Mg and 80% of Si have been leached from the profile, in agreement with observations reported in Golighlty (1981) and Butt and Cluzel (2013) (RC in Fig. 7). A significant increase of Mg aqueous concentration is observed between the goethite and saprolite horizons. Fe and Ni are scarcely leached out of the system.

The model results suggest that sorption of Ni onto the goethite surface can explain the amount of Ni found in the goethite at Moa. In the model, however, sorption of Ni occurs only on goethite in contact with serpentine II. This distribution, in accordance with the observations of Dublet et al. (2015) of a regular decrease in bulk Ni content upwards in the profile and of Soler et al. (2008) in the goethite horizon of Loma de Hierro deposit, is directly linked to the evolution of pH. Sorption of Ni onto goethite depends on pH, and as can be seen in Fig. 6, when pH decreases below 7, sorption of Ni significantly decreases achieving values around 10% or less at pH 5 (Dublet et al. 2015). In natural conditions, however, goethite particles with Ni sorbed onto their surface might flocculate or form aggregates. For goethite, the point of zero charge (PZC) is between pH = 6.5 to 9.5 (Strauss et al. 1997; Gaboriaud and Ehrhardt, 2002). At the PZC, a dispersion of particles exhibits its maximum flocculation rate. In the profile, this range of pH is encountered in the saprolite, towards the limonitic horizon, where it might well favor the flocculation/aggregation of the goethite particles that could prevent desorption of Ni.

In the model, nesquehonite is always subsaturated (saturation indices below -2) while quartz presents saturation indices about 0.7 in the partially serpentinized peridotite horizon and close to 0.4 in the saprolite horizon.

Sensitivity analyses

Different cases have been investigated to evaluate the effect of the uncertainty of some key parameters on the model results. As shown in Table 6, sensitivity analyses explore the effect of not considering sorption of Ni onto goethite (*No_ads* case), of using different chemical compositions for serpentine II (*Srp II** and *Srp II*$^{\$}$ cases), of considering faster dissolution rates of Fo_{90} and En_{90} (*Rate* case), of considering a smaller carbonate concentration (*Less_carb* case), or allowing the precipitation of quartz (*Qt* case).

In the ***No_ads*** sensitivity analysis, the formation of surface species onto goethite is not considered. After 10^6 years of elapsed time, the same horizons developed as in the RC, with a goethite horizon with pH 4.5, a saprolite horizon with serpentine II and goethite at pH 8.3, and a partially weathered peridotite with serpentine I and II and goethite at pH 8.6. Mg and Si are also significantly leached (Fig. 7) but as shown in Fig. 8, the saprolite horizon is thicker than in the RC. This is due to the fact that, on one hand, all Ni is available to precipitate in Srp II whereas in RC, sorption of Ni was dominant and Srp II formed once the goethite surface was saturated, and on the other, the pH of porewater is not affected by the (de)protonation of goethite. In the RC, pH was lower in the saprolite horizon because sorption of Ni

displaced H^+ from the goethite surface, while in the *No_ads* case, the pH in the saprolite horizon is maintained at 8.3, the same pH that is achieved in the RC when goethite becomes saturated in Ni (Fig. 9). To account for the variability of compositions of Srp II observed in the field, two more chemical compositions have been used in the sensitivity analyses ***Srp II**** and ***Srp II$*** (Table 4). These two Srp II have been chosen as they are the compositions having the lowest and the highest solubility constants, respectively. Results indicate that the same main processes are occurring as in the RC (Fig.7, Fig. 9), but that the composition of Srp II affects the final distribution of the profile horizons (Fig. 8). On one hand, the thickness of the saprolite horizon, dominated by Srp II, decreases as the solubility of this mineral increases (*Srp II$* in Fig. 8). On the other hand, the amount of leached Ni is higher in the sensitivity case *Srp II**, that is, the one considering the Srp II with the lowest Ni content (Table 4).

In the ***Rate*** case**,** the reactive areas of Fo_{90} and En_{90} are set equal to 0.1 m^2/g to obtain dissolution rates of Fo_{90} and En_{90} that are 200 and 20 times faster, respectively, than in the RC. Results show that these faster dissolution rates increase the amounts of Si, Ni, Mg and Fe released, which also leads to increased goethite precipitation and Ni adsorption. Fo_{90} and En_{90} are completely consumed before (1000 and 1.5×10^5 years respectively), without further effects on laterite formation. After 10^6 years of elapsed time, differences with the RC are minor (Fig. 7-9).

In the sensitivity analysis ***Less_carb***, only the infiltrating rain water is in equilibrium with atmospheric O_2(g) and CO_2(g). The model reproduces a case in which the system is fully saturated (water table at the surface), limiting the input of O_2(g) and CO_2(g) to the system (Butt and Cluzel 2013). As shown in Fig. 8, the advancement of the weathering front after 10^6 years is small compared to the RC. The main reason for such big difference is the availability of carbonate, which affects pH. In this sensitivity analysis, the lack of dissolved CO_2(g) does not buffer pH and, as a result of Srp I dissolution, pH goes up quickly and the solution becomes saturated with respect to primary minerals (Fig. 8). In the RC, where atmospheric CO_2(g) is always available in the column, dissolution of CO_2(g) provides enough acidity to buffer the increase in pH caused by silicate mineral dissolution. This observation agrees with Golightly (1981) that identified carbonate as one of the principal agents of weathering. When carbonate is not available, the solubility of serpentine is lower and the reaction front moves slowly. As a consequence, in 10^6 years of elapsed time, Mg and Si leaching is not as important as for the other cases (Fig. 7) and pH is around 10 (Fig. 9). The *Less_carb* and RC results suggest that the aqueous carbonate concentration is, in fact, an

important key parameter controlling the rate of laterite formation. Any phenomena preventing CO_2(g) equilibration with porewater would lessen laterite profile development.

As reported previously in the RC, saturation indices of quartz indicated a slight oversaturation, especially along the saprolite and peridotite horizons. In the ***Qt*** sensitivity analysis, quartz is allowed to precipitate according to local equilibrium. Results show that quartz precipitation is significant because Si is preferentially retained as quartz rather than being incorporated in Srp II and, consequently, the weathering front is advancing faster. After 10^6 years of elapsed time, the profile presents two different horizons (Fig. 8). The first 11.5 m are of goethite, with a porosity of 91% and a pH of 4.5; and the other 75 m are composed of 43% (in vol.) of quartz and 9 % (in vol.) of goethite with a porosity of 48% and a pH of 6 (Fig. 9). All Mg and nearly 40% of Ni have been leached from the system, while leaching of Si is reduced to 15% (Fig. 7). Microcrystalline quartz in laterite profiles has been reported in some profiles (e.g. Golightly 1981; Tauler et al. 2009; Villanova-de-Benavent et al. 2014) and observed in cases with small lixiviation rates (Butt and Cluzel 2013), but it does not form in those cases where weathering rate is fast (Golightly 2010). In the RC, quartz saturation indicates its possible precipitation but the results obtained when quartz is allowed to precipitate are not consistent with field observations. An explanation to this might be found in the value of the saturation indices calculated for quartz, that were not higher than 0.7. These small saturation indices might not be enough to overcome a kinetic barrier for the precipitation of quartz. Instead of the precipitation of quartz under local equilibrium, the precipitation of an amorphous phase such as SiO_2(am), or a kinetically controlled precipitation of quartz should have been considered.

Conclusions

This paper presents a reactive transport model of the formation of the Punta Gorda Ni-laterite deposit of Moa mining district (northeast of Cuba). The model is based on the conceptual model of Butt and Cluzel (2013), according to which laterite deposits form due to a continuous weathering of a partially serpentinized peridotite under tropical climate. Numerical model considers a 1D column of 88 m length initially composed of Fo_{90}, En_{90}, Srp I and Mag. Due to the interaction with rainwater, these primary minerals dissolve, and a Fe(III) and Ni bearing serpentine (Srp II) and goethite precipitate. Ni is allowed to sorb onto goethite.

Although some of the assumptions made in the numerical model are simplifications of the real system, results of the model are consistent with the conceptual model about the formation of oxide type Ni-laterite deposits:

- After 10^6 years of elapsed time, simulations reproduce the three main horizons observed in the field: a) a thick limonite horizon, at the top of the profile, composed of goethite, b) a narrow saprolite horizon, in the middle, composed of Srp II and Gth, and c) a partially weathered serpentinized peridotite horizon, at the bottom, in which Srp I, Srp II and Gth coexist.
- Simulations show the increase of porosity from values close to 5% at the bottom to values close to 90% at the top of the profile, due to the dissolution of silicate minerals and the pH increase from 4.5 at the top (rainwater pH) to values close to 8.6 at the bottom, being 8.3 at the saprolite horizon.
- Sorption of Ni onto goethite can explain the field observations. Ni sorption onto goethite is linked to pH, showing its maximum in the saprolite horizon, as observed in the field. Sorption onto goethite in the limonite horizon decreases because of the acidic pH, which displaces Ni^{2+} from the surface sites. In the serpentinized peridotite horizon, sorption is negligible because Ni is preferentially retained in Srp I.
- During the laterization process, Mg and Si are leached out the system, while Fe and Ni are conserved.

This simulation exercise has been useful not only to identify but also, to quantify, the effect that some variables can have on the formation of laterites:

- The saprolite reaction front does not advance while there is Srp I in the system.
- Protonation/desprotonation of goethite surface exerts a significant control on porewater pH as it increases acidic pH of entering rainwater but also decrases pH of saprolite horizon porewater to values below 8.3, preventing the development of saprolite horizon. Nevertheless, this control finishes when goethite surface sites saturate.
- Aqueous carbonate concentration is an important key parameter as it controls the rate of laterization process, with laterization increasing with carbonate concentration. This is due to carbonic acid buffering capacity, which buffers the increase of pH due to silicate dissolution.
- Forsterite is the main mineral providing Ni to the system. The dissolution rate of Fo and En affects the thicknesses of the different horizons.

- Serpentine II composition influences the development of laterite profile, from two perspectives: serpentine II poor in Ni causes an increase of the % of Ni leached after 10^6 years of elapsed time and since composition determines the solubility constant of serpentine, the more soluble the serpentine is, the narrower the saprolite horizon is. In any case, its effect is minor and must be further evaluated.
- Precipitation of quartz significantly enhances the formation of the limonitic horizon and inhibits the formation of the saprolite horizon. The inclusion of quartz or even an amorphous silica phase must be evaluated in more details.

Results of this study provide new valuable insights to the understanding of the differences between Ni-laterite deposit types and show the capabilities of reactive transport simulations to test and validate conceptual models. The model could be improved by increasing either the complexity of the geochemical system (more minerals, solid solutions, incorporation of Ni into goethite structure,…) or the physical system (2D or 3D, matrix diffusion to simulate corestones structures, mineral heterogeneity…). Finally, investigations on the PZC of goethite under the hydrochemical conditions of the Moa profile would account for flocculation of particles that may preserve Ni all along the goethite horizon.

ACKNOWLEDGEMENTS

This research has been financially supported by FEDER Funds, the Spanish projects CGL2009-10924 and CGL2012-36263 and Catalan project 2014-SGR-1661. We are grateful to Prof. J.P. Golightly, Prof. G.Beaudoin, M.Cathelineau and an anonymous reviewer for their careful reviews and constructive criticism of the original manuscript.

Conflict of interest

The authors declare that they have not conflict of interest.

References

Aiglsperger, T., Proenza, J.A., Lewis, J.F., Labrador, M., Svojtka, M., Rojas-Purón, A., Longo, F., Ďurišová, J. (2016): Critical metals (REE, Sc, PGE) in Ni laterites from Cuba and the Dominican Republic. Ore Geol Rev 73: 127-147. DOI:10.1016/j.oregeorev.2015.10.010

Arai, Y. (2008) Spectroscopic evidence for Ni(II) surface speciation at the iron oxyhydroxides-water interface. Environ Sci Technol: 1151–1156

Beukes JP, Giesekke EW, Elliott W (2000) Nickel retention by goethite and hematite. Miner Eng 13: 1573-1579

Bertolo R, Hirata R, Sracek O (2006) Geochemistry and geochemical modeling of unsaturated zone in a tropical region in Urânia, Sao Paulo state, Brazil. J Hydrol 329: 49– 62

Brunauer S, Emmett PH, Teller E (1938) Adsorption of gases in multimolecular layers. J Am Chem Soc 60: 309-319

Bryce AL, Kornicker WA, Elrerman AW (1994) Nickel adsorption to hydrous ferric oxide in the presence of EDTA: effects of component addition sequence. Environ Sci Technol 28: 2353-2359

Buerge-Weirich D, Hari R, Xue H, Behra P, Sigg L (2002) Adsorption of Cu, Cd, and Ni on goethite in the presence of natural groundwater ligands. Environ Sci Technol 36: 328-336

Butt CRM, Cluzel D (2013) Nickel Laterite Ore Deposits: Weathered Serpentinites. Elements 9:123-128. doi: 10.2113/gselements.9.2.123

Carvalho-e-Silva MLM, Partiti CSM, Enzweiler J, Petit S, Netto SM, De Oliveira SMB (2002) Characterization of Ni-containing goethites by Mössbauer spectroscopy and other techniques. Hyperfine Interact 142: 559–576

Carvalho-e-Silva MLM, Ramos AY, Nogueira Tolentino HC, Enzweiler J, Netto SM, Martins Alves MC (2003) Incorporation of Ni into natural goethite: An investigation by X-ray absorption spectroscopy. Am Mineral 88: 876–882. 0003-004X/03/0506–87605.00 876

Cathelineau M, Quesnel B, Gautier P, Boulvais P, Couteau C, Drouillet M (2016) Nickel dispersion and enrichment at the bottom of the regolith: formation of pimelite target-like ores in rock block joints (Koniambo Ni deposit, New Caledonia) Miner Deposita 51:271-282. doi: 10.1007/s00126-015-0607-y

Corbella M, Ayora C, Cardellach E (2004) Hydrothermal mixing, carbonate dissolution and sulfide precipitation in Mississippi Valley-type deposits. Miner Deposita 39: 344–357. doi: 10.1007/s00126-004-0412-5.

Cornell RM (1991) Simultaneous incorporation of Mn, Ni and Co in the goethite (α-FeOOH) structure. Note. Clay Miner 26: 427-430

Coughlin BR, Stone AT (1996) Nonreversible adsorption of divalent metal ions (Mn^{II}, Co^{II}, Ni^{II}, Cd^{II} and Pb^{II}) onto goethite: effects of acidification, Fe^{II} addition, and picolinic acid addition. Environ Sci Technol 29: 2445-2455

Davis JA, Kent DB (1990) Surface complexation modeling in aqueous geochemistry. In: Hochella MF, White AF (eds) Reviews in Mineralogy, Mineral-Water Interface Geochemistry, 23, Mineralogical Society of America, Washington, DC, pp. 177–260

De Keijser ThH, Langford JJ, Mittemeijer EJ, Vogels ABP (1982) Use of the Voigt function in a single-line method for the analysis of X-ray diffraction line broadening. J Appl Crystallogr : 308-314

Dublet G, Juillot F, Morin G, Fritsch E, Fandeur D, Ona-Nguema G, Brown Jr GE (2012) Ni speciation in a New Caledonian lateritic regolith: A quantitative X-ray absorption spectroscopy investigation. Geochim Cosmochim Acta 95: 119–133

Dublet G, Juillot F, Morin G, Fritsch E, Fandeur D, Brown Jr GE (2015) Goethite aging explains Ni depletion in upper units of ultramafic lateritic ores from New Caledonia. Geochim Cosmochim Acta 160: 1-15

Fan R, Gerson AR (2011) Nickel geochemistry of a Philippine laterite examined by bulk and microprobe synchrotron analyses. Geochim Cosmochim Acta 75: 6400–6415

Fletcher RC, Brantley SL (2010) Reduction of bedrock blocks as corestones in the weathering profile: observations and model. Am J Sci 310: 131–164. doi: 10.2475/03.2010.01

Fletcher RC, Buss HL, Brantley SL (2006) A spheroidal weathering model coupling porewater chemistry to soil thicknesses during steady-state denudation. Earth Planet Sc Lett 244: 444–457.

Fischer L, Brümmer GW, Barrow NJ (2007) Observations and modelling of the reactions of 10 metals with goethite: adsorption and diffusion processes. Eur J Soil Sci 58: 1304–1315. doi: 10.1111/j.1365-2389.2007.00924.x

Foster L, Eggleton RA (2002) The Marlborough nickel laterite deposits. In: Roach I.C. ed. 2002. Regolith and Landscapes in Eastern Australia 33-36. CRC LEME

Freyssinet Ph, Butt CRM, Morris RC (2005) Ore-forming processes related to lateritic weathering: Econ Geol 100th Anniv Vol: 681-722

Galí S, Proenza JA, Labrador M, Tauler E, Melgarejo JC (2007) Numerical modeling og oxide-type Ni laterite deposits: preliminary results. In CJ Andrew et al. (eds) Digging Deeper Proceedings of the ninth bienal SGA meeting. Dublin (Ireland), 1385-1388

Gamsjäger H, Bugajski J, Gajda T, Lemire RJ, Preis W (2005) Chemical thermodynamics of Nickel, Nuclear Energy Agency Data Bank, Organisation for Economic Co-operation and Development, Ed.,

vol. 6, Chemical Thermodynamics, North Holland Elsevier Science Publishers B. V., Amsterdam, The Netherlands.

Gehring AU, Fischer H, Louvel M, Kunze K, Weidler PG (2009) High temperature stability of natural maghemite: a magnetic and spectroscopic study. Geophys J Int 179, 1361–1371. doi: 10.1111/j.1365-246X.2009.04348.x

Giffaut E, Grivé M, Blanc Ph, Vieillard Ph, Colàs E, Gailhanou H, Gaboreau S, Marty N, Madé B, Duro L (2014) Andra thermodynamic database for performance assessment: ThermoChimie. Appl Geochem 49: 225-236

Gleeson SA, Butt CR, Elias (2003) Nickel laterites: a review. SEG News 54: 11–18.

Goodfellow BW, Hilley GE, Schulz MS (2011) Vadose zone controls on weathering intensity and depth: Observations from grussic saprolites Appl Geochem 26: S36–S39. doi:10.1016/j.apgeochem.2011.03.023

Golightly JP (1981) Nickeliferous laterite deposits. Econ Geol, 75th anniversary volume 710-735

Golightly JP, Plamondon M, Srivastava RM (2008) 43-101F1 technical report on the Camarioca Norte and Camarioca Sur nickel laterite properties in Cuba (www.sedar.com Sherritt International filed May 9 2008).

Golightly JP (2010) Progress in understading the evolution of nickel laterites. Soc Eco Geo Spe Pub 15: 451-485

Golightly JP, Arancibia ON (1979) The chemical composition and infrared spectrum of nickel- and iron-substituted serpentine from a nickeliferous laterite profile, Soroako, Indonesia. Can Mineral 17: 719–728

Hayes KF, Leckie JO (1987) Modeling ionic strength effects on cation adsorption at hydrous oxide/solution interfaces. J Colloid Interf Sci 115: 564-572

Hewawasam T, von Blanckenburg F, Bouchez J, Dixon JL, Schuessler JA, Maekeler R. (2013) Slow advance of the weathering front during deep,supply-limited saprolite formation in the tropical Highlands of Sri Lanka Geochim Cosmochim Acta 118: 202–230.

Klug HP, Alexander LE (1962) X-Ray Diffraction Procedures for polycrystalline and amorphous materials (Chapter 9). New York. John Wiley and Sons. Inc.

Königsberger E, Königsberger LC, Gamsjäger H (1999) Low temperature thermodynamic model for the system Na_2CO_3-$MgCO_3$-$CaCO_3$-H_2O. Geochim Cosmochim Acta 63: 3105-3119

Lambiv Dzemua G, Gleeson S A, Schofield P F (2013) Mineralogical characterization of the Nkamouna Co–Mn laterite ore, southeast Cameroon. Miner Deposita 48: 155-171. DOI 10.1007/s00126-012-0426-3

Langford JL (1978) A rapid method for analyzing the breaths of diffraction and spectral lines using the Voigt function. J Appl Crystallogr 11: 10-14

Lasaga AC (1998) Kinetic Theory in the Earth Sciences. Princeton. University Press, Princeton

Lavaut W (1998) Tendencias geológicas del intemperismo de las rocas ultramáficas en Cuba oriental. Minería y Geología 15: 9–16.

Lebedeva MI, Fletcher RC, Balashov VN, Brantley SL. (2007) A reactive diffusion model describing transformation of bedrock to saprolite. Chem Geol 244: 624–645

Lewis JF, Draper G, Proenza JA, Espaillat J, Jimenez J (2006) Ophiolite-related ultramafic rocks (serpentinites) in the Caribbean Region: A review of their occurrence, composition origin, emplacement and Ni-laterite soils formation. Geol Acta 4: 237-263

Linchenat A, Shirakova I (1964) Individual characteristics of nickeliferous iron (laterite) deposits of the northeast part of Cuba (Pinares de Mayari, Nicaro and Moa). 24th International Geological Congress, Montreal, Part 14, Section 14, 172–187

Louër D, Aufrédic JP, Langford JL, Ciosmak D, Niepce JC (1983) A precise determination of the shape, size and distribution of size of crystallites in zinc oxide by X-ray line-broadening analysis. J Appl Crystallogr 16: 183-191

Manceau A, Schlegel ML, Musso M, Sole VA, Gauthier C, Petit PE, Trolard F (2000) Crystal chemistry of trace elements in natural and synthetic goethite. Geochim Cosmochim Acta 64: 3643-3661

Marchesi C, Garrido CJ, Godard M, Proenza JA, Gervilla F, Blanco-Moreno J (2006) Petrogenesis of highly depleted peridotites and gabbroic rocks from the Mayarí-Baracoa Ophiolitic Belt (eastern Cuba). Contrib Mineral Petr 151: 717–736

Marcussen H, Holm PE, Strobel BW, Hansen HCB (2009) Nickel sorption to goethite and montmorillonite in presence of citrate. Environ Sci Technol 43: 1122-1127

Moore J, Lichtner PC, White AF, Brantley SL (2012) Using a reactive transport model to elucidate differences between laboratory and field dissolution rates in regolith. Geochim et Cosmochim Acta 93: 235–261

Morgan B, Wilson SA, Madsen IC, Gozukara YM, Habsuda J (2015) Increased thermal stability of nesquehonite ($MgCO_3 \cdot 3H_2O$) in the presence of humidity and CO_2: Implications for low-temperature CO_2 storage. Int J Greenh Gas Con 39: 366–376. doi:10.1016/j.ijggc.2015.05.033

Navarre-Sitchler A, Steefel CI, Sak PB, Brantley SL (2011) A reactive-transport model for weathering rind formation on basalt. Geochim Cosmochim Acta 75: 7644-7667 doi:10.1016/j.gca.2011.09.033

Oliveira SMB, Partiti CSM, Enzweiler J (2001) Ochreous laterite: a nickel ore from Punta Gorda, Cuba. J S Am Earth Sci 14: 307-317

Palandri JL, Kharaka YK (2004) A compilation of rate parameters of water-mineral interaction kinetics for application to geochemical modelling, U.S. Geological Survey, Open file report 2004-1068

Pelletier B (1996) Serpentines in nickel silicate ore from New Caledonia. Australasian Institute of Mining and Metallurgy Publication Series - Nickel conference, Kalgoorlie (Western Australia) 6/96 197–205

Power IM, Wilson SA, Dipple GM (2013) Serpentine carbonation for CO_2 sequestration. Elements 9: 115-121. doi: 10.2113/gselemnts.9.2.115

Proenza JA, Gervilla F, Melgarejo JC, Bodinier JL (1999) Al- and Cr-rich chromitites from the Mayarí–Baracoa Ophiolitic Belt (Eastern Cuba): consequence of interaction between volatile-rich melts and peridotite in suprasubduction mantle. Econ Geol 94: 547–566

Proenza JA, Tauler E, Melgarejo JC, Galí S, Labrador M, Marrero N, Pérez-Melo N, Rojas-Purón AL, Blanco-Moreno JA (2007) Mineralogy of oxide and hydrous silicate Ni-laterite profiles in Moa Bay area, northeast Cuba. In: Andrew et al. (eds.), Digging Deeper, Irish Association for Economic Geology, Dublin, Ireland. 2: 1389-1392

Quesnel B, Boulvais P, Gautier P, Cathelineau M, Cédric MJ, Dierick M, Agrinier P, Drouillet M (2016) Paired stable isotopes (O, C) and clumped isotope thermometry of magnesite and silica veins in the New Caledonia Peridotite Nappe. Geochim Cosmochim Acta 183: 234-249.

Rajapaksha AU, Vithanage M, Weerasooriya R, Dissanayake CB (2012) Surface complexation of nickel on iron and aluminum oxides: a comparative study with single and dual site clays. Colloid Surface A 405: 79-87

Richter A, Brendler V, Bernhard G (2005) Blind prediction of Cu(II) sorption onto goethite: Current capabilities of diffuse double layer model. Geochim et Cosmochim Acta 69: 2725-2734

Richter A, Brendler V (2008) Blind Prediction and Parameter Uncertainty – A Sorption Test Case. In M. Barnett O, Kent BD (eds) Developments in Earth and Environmental Sciences 7, Chapter 10

Rojas-Purón A, Simões Angélica R, Orozco-Melgar, O (2012) Identificación mineralógica de los óxidos de manganeso del yacimiento laterítico Punta Gorda, Moa, Cuba. Minería y Geología, 28: 1-26

Roqué-Rosell J, Mosselmans JFW, Proenza JA, Labrador M, Galí S, Atkinson KD, Quinn PD (2010) Sorption of Ni by “lithiophorite–asbolane” intermediates in Moa Bay lateritic deposits, eastern Cuba. Chem Geol 275: 9-18.

Rose AW, Bianchi-Mosquera GC (1993) Adsorption of Cu, Pb, Zn, Co, Ni and Ag on goethite and hematite. A control on metal mobilization from Red Beds into stratiform copper deposits. Econ Geol 88: 1226-1236

Singh B, Sherman DM, Gilkes RJ, Wells MA, Mosselmans JFW (2002) Incorporation of Cr, Mn and Ni into goethite (α-FeOOH): mechanism from extended X-ray absorption fine structure spectroscopy. Clay Miner 37: 639–649

Soler JM (2013) Reactive transport modeling of concrete-clay interaction during 15 years at the Tournemire Underground Rock Laboratory. Eur J Mineral 25: 639–654

Soler JM, Cama J, Galí S, Melendez W, Ramirez A, Estanga J (2008) Composition and dissolution kinetics of garnierite from the Loma de Hierro Ni-laterite deposit, Venezuela. Chem Geol 249:191-202

Soler JM, Lasaga AC (1996) A mass transfer model of bauxite formation. Geochim Cosmochimi Acta 60: 4913-4931

Soler JM, Lasaga AC (1998) An advection-dispersion-reaction model of bauxite formation. J Hydrol 209: 311-330

Steefel CI (2009) CrunchFlow. Software for modeling multicomponent reactive flow and transport. User’s manual. Lawrence Berkeley National Laboratory, Berkeley

Steefel CI and Lasaga AC (1994) A coupled model for transport of multiple chemical-species and kinetic precipitation dissolution reactions with application to reactive flow in single-phase hydrothermal systems. Am J Sc 294: 529–592

Steefel CI, Appelo CAJ, Arora B, Jacques D, Kallbacher T, Kolditz O, Lagneau V, Lichtner C, Mayer KU, Meeussen JCL, Molins S, Moulton D, Shao H, Simunek J, Spycher N, Yabusaki SB, Yeh GT (2015) Reactive transport codes for subsurface environmental simulation. Computat Geosci 19: 445–478. doi: 10.1007/s10596-014-9443-x

Strauss R, Brümmer GW and Barrow NJ (1997) Effects of crystallinity of goethite: I. Preparation and properties of goethites of differing crystallinity. Eur J Soil Sci 48: 87-99

Tauler E, Proenza JA, Galí S, Lewis JF, Labrador M, García-Romero E, Suárez M, Longo F, Bloise G (2009) Ni-sepiolite-falcondote in garnierite mineralization from the Falcondo Ni-laterite deposit, Dominican Republic. Clay Miner 44:435-454. DOI: 10.1180/claymin.2009.044.4.435

Thorne RL, Roberts S, Herrington R (2012) Climate change and the formation of nickel laterite deposits. Geology 40: 331-334

Trivedi P, Axe L (2001) Ni and Zn sorption to amorphous versus crystalline iron oxides: macroscopic studies. J Colloid Interf Sci 244: 221–229. doi:10.1006/jcis.2001.7970

Trivedi P, Axe L, Dyer J (2001) Adsorption of metal ions onto goethite: single-adsorbate and competitive systems. Colloid Surface A 191: 107–121

Ulrich M, Muñoz M, Guillot S, Cathelineau M, Picard C, Quesnel B, Boulvais P, Couteau C. (2014) Dissolution–precipitation processes governing the carbonation and silicification of the serpentinite sole of the New Caledonia ophiolite. Contrib Mineral Petr 167:952. doi: 10.1007/s00410-013-0952-8

Veneklaas EJ (1990) Nutrient fluxes in bulk precipitation and throughfall in two montane tropical rain forests, Colombia. J Ecol 78: 974-992

Villanova-de-Benavent C, Proenza JA, Galí S, García-Casco A, Tauler, E, Lewis JF, Longo F (2014) Garnierites and garnierites: Textures, mineralogy and geochemistry of garnierites in the Falcondo Ni-laterite deposit, Dominican Republic. Ore Geol Rev 58, 91–109

Villanova-de-Benavent C, Domènech C, Tauler C, Galí S, Tassara S, Proenza JA (2016a) Fe-Ni-Rich Serpentines from the Saprolite Horizon of Caribbean Ni-Laterite Deposits: a New insights from Thermodynamic Calculations. Miner Deposita. DOI 10.1007/s00126-016-0683-7.

Villanova-de-Benavent C, Nieto F, Viti C, Proenza JA, Galí S, Roqué-Rosell J (2016b) Ni-phyllosilicates (garnierites) from the Falcondo Ni-laterite deposit (Dominican Republic): Mineralogy, nanotextures, and formation mechanisms by HRTEM and AEM. Am Mineral 101, 1460–1473.

Wells MA, Ramanaidou ER, Verrall M, Tessarolo C (2009) Mineralogy and chemical chemistry of garnierites in the Goro lateritic nickel deposit, New Caledonia. Eur J Mineral 21:467–483.

Whitney DL Evans BW (2010) Abbreviations for names of rock-forming minerals. Am Mineral 95: 185-187.

Williams MR, Fisher TR, Melack JM (1997) Chemical composition and deposition of rain in the central amazon, Brazil. Atmos Environ 31: 207-217

Wolery TJ (1992) EQ3NR, a computer program for geochemical aqueous speciation-solubility calculations: Theoretical manual, user's guide and related documentation (Version 7.0). Publ UCRL-MA-110662 Pt III, Lawrence Livermore Lab, Livermore Calif.

Xu Y, Axe L, Boonfueng T, Tyson TA, Trivedi P, Pandya K (2007) Ni(II) complexation to amorphous hydrous ferric oxide:An X-ray absorption spectroscopy study. J Colloid Interf Sci 314: 10–17

Figure captions

Fig.1 Location and simplified geological map of the Moa Bay mining area (Cuba) showing the location of the Punta Gorda Ni-laterite deposit. Modified from Marchesi et al. (2006).

Fig. 2 Schematic representation of the studied profile of the Punta Gorda Ni-laterite deposit (a) and mineral composition of the analyzed samples (b). Mineral abbreviations taken from Whitney and Evans (2010) (Fo: forsterite, En: enstatite, Srp: serpentine, Mgh: maghemite, Gth: goethite, Hem: hematite, Gib: gibbsite, Qz: quartz), except pyrochroite (Prc). Modified from Galí et al. (2007).

Fig. 3 X-Ray diffraction diagram of sample M4 from Punta Gorda. Agreement index Rwp = 10.31. Triangles at bottom are the position of the reflections used for calculating D_{hkl} values from measured 2θ and $FWHM_{hkl}$ values.

Fig. 4 Evolution of the amount of mineral (in wt.%) (areas) and of the amount of Ni sorbed onto goethite (in wt.% of Ni in goethite) (solid line) and porosity in the profile at initial time (0 y) and at different model elapsed times (from 10^3 to 10^6 years) for the Reference case.

Fig. 5. pH distribution at the profile at different time steps for the Reference case.

Fig. 6 Distribution of Mg, Si, Fe and Ni aqueous concentration (a), goethite surface species (b), and pH (c) along the modeled profile after 1My of elapsed time.

Fig. 7 Amount of Mg, Si and Ni (in wt.%) leached out from the modelled profile after 10^6 years of elapsed time for the RC (Reference case) and the different sensitivity analyses reported: *No_ads*, without considering sorption of Ni onto goethite, *Srp II** and *Srp II*$^\$$,considering different serpentine compositions, see Table 4, *Rate*, considering faster dissolution rates of enstatie and forsterite, *Less_carb*, considering a smaller concentration of carbonate and *Qt*, allowing quartz precipitation.

Fig. 8 Distribution of the horizons along the modelled profile after 10^6 years of elapsed time for the RC (Reference case) and the different sensitivity analyses reported (same abbreviations from Fig.7).

Fig. 9 Evolution of pH along the modelled profile after 10^6 years of elapsed time for the Reference case and the different sensitivity analyses reported (same abbreviations from Fig.7).

Table captions

Table 1 pH, Eh (in V) and total concentration of components of rainwater and initial porewater (in mol/L). Mineral abbreviations from Whitney and Evans (2010)

Table 2 Initial mineral composition considered in the model.

Table 3 Solubility constants at 25ºC of the pure end-member phases used to calculate solubility constants of solid solutions used in the simulations. Mineral abbreviations from Whitney and Evans (2010).

Table 4 Solubility constants at 25ºC calculated for the solid solutions used in the simulations.

[*$]serpentines II used in the sensitivity cases. Mineral abbreviations from Whitney and Evans (2010).

Table 5 Equilibrium constants for goethite surface reactions used in the calculations.

Table 6 Summary of the main differences between the Reference case and the sensitivity analyses.

authors

Click here to download Authors' Response to Reviewers' Comments answers to reviewers_4thdrevision.pdf

Reactive transport model of the formation of oxide type Ni-laterite profiles (Punta Gorda, Moa Bay, Cuba)

Cristina Domènech, Salvador Galí, Cristina Villanova-de-Benavent, Josep M. Soler and Joaquín A. Proenza

Ref.: Ms. No. MIDE-D-16-00020R3

Answers to the editor-in-chief Prof.Georges Beaudoin

We appreciate the modifications proposed by Prof. G.Beaudoin. We have accepted all them, except in the following cases, where an alternative text or a response to the reviewer has been proposed. Line numbers refer to the pdf document revised by Prof. G.Beaudoin.

Line 19. "oxide type Ni-laterite deposit". We have chosen to maintain oxide type Ni-laterite deposit, but we have carefully checked the text to make it uniform.

Line 25. "Percentages of Ni" has been changed by "the weight percent of Ni".

Line 29. "while the effect of serpentine II composition or dissolution mineral rates is minor" has been changed by "while the effect of the composition of secondary serpentine or of mineral dissolution rates is minor".

Line 47. "under favorable climatic and topographic conditions" has been changed by "under favorable topography and climatic conditions".

Line 84. "Ni sorbs onto goethite forming inner sphere mononuclear bidentate complexes (Trivedi et al. 2001; Xu et al. 2007)," has been changed by "Ni sorbs onto goethite forming inner-sphere mononuclear bidentate complexes (Trivedi et al. 2001; Xu et al. 2007)".

Inner-sphere surface complexes is the name of those surface complexes in which there is a direct bond between the surface and the adsorbed species, in contrast to the outer-sphere surface complexes in which there is a shell of water molecules between the surface and the complex.

Line 86. Sorption of Ni onto goethite has been modelled by considering Langmuir isotherms (Trivedi et al. 2001), a Diffuse Layer Model (Bryce et al. 1994; Buerge-Weirich et al. 2002; Marcussen et al. 2009; Rajapaksha et al. 2012) or a Triple Layer Model (Coughlin and Stone 1995).

Why is this important? Delete if only information

We prefer to leave this text because it introduces the different models that have been used in the literature to explain sorption of Ni onto goethite. In the modelling exercise we have used that of Marcussen et al. (2009).

Line 98. "Differential thermal gravimetric (DTA-TGA) and EXAFS analyses" has been changed by "Differential thermal (DTA), thermal gravimetric (TGA) and EXAFS analyses" because De Carvalho et Silva et al. (2002, 2003) performed all these types of analyses.

Line 120. Spheroidal weathering means the "onion type" weathering observed to occur in some granites. We have removed it from the text, as it did not provide relevant information.

Line 130. "Navarre-Sitchler et al. (2011) used the reactive coupled transport model CrunchFlow to simulate". Commas have not been added given that reactive coupled transport model is a term usually used.

Line 132. "mineral kinetics dominated over transport, and that weathering front rate was controlled by the rate at which porosity was created" has been changed by "mineral reaction kinetics dominated over transport, and that the advance of the weathering front was controlled by the rate at which porosity was created".

Line 136. "Moreover, they had to reduce the laboratory rates (by decreasing the surface reactive areas) to fit the field observations" has been changed by "Moreover, they had to use reduced reaction rates, compared with rates from laboratory studies, to fit the field observations".

Line 137. "They concluded that reactive transport models can be used to understand the long-lived (10^6 years) mineral weathering processes given that they can cope with simultaneous processes that do not behave linearly" has been changed by "They concluded that reactive transport models can be used to understand the long-lived (10^6 years) mineral weathering processes given that they consider the simultaneous non-linear processes".

Line 149. The word "horizons" has not been changed by laterite facies. It is a common and accepted word that is used in the whole document. We have added the word "laterite" before "horizons".

Line 151. "a first modeling exercise" has not been changed by "modeling experiments" as we have not done experiments but numerical calculations.

Line 204. "impregnated by plagioclase, which was exposed to the surface during the late Miocene (≈ 10^7 years) (Lewis et al. 2006)." has been changed by "including plagioclase-rich bodies, which was exposed to the surface during the late Miocene (≈ 10^7 years; Lewis et al. 2006).

Line 207. "and lizardite 2H1 is less crystalline and presents many stacking faults" has been changed by "whereas lizardite 2H1 is less crystalline and presents many stacking faults in its structure".

Line 262. "Ni may be further leached from goethite and form garnierite deeper in the profile" has been changed by "Ni may be leached from goethite to garnierite deeper in the profile".

Line 278. "and transport processes under fully saturated flow conditions and different temperatures (Steefel et al. 2015)." has been changed by "and transport processes under fully saturated flow conditions and variable temperature (Steefel et al. 2015)".

Line 281. "However, if rates" has been changed by "However, if reaction rates".

Line 287. "Total porosity (ϕ_T) may be updated" has been changed by "Total porosity is updated".

Line 326. "A diffusion coefficient of 1.0×10^{-10} m^{-2} s^{-1} is considered" has been changed by "a water diffusion coefficient for solutes of 1.0×10^{-10} m^{-2} s^{-1} is used".

Line 352. "Additional log K values (e.g. forsterite), are calculated from published ΔG_r^o (e.g. Ni_2SiO_4) or estimated ΔG_f values (e.g. Fe(III)-lizardite, Villanova-de-Benavent et al. 2016a)." has been changed by "Additional log K values (e.g. forsterite) are calculated from ΔG_r^o or ΔG_f values from literature (Villanova-de-Benavent et al. 2016a)."

Line 441. "in order to simulate the effect of unsaturated flow, once the model starts," has been changed by "In order to simulate the effect of unsaturated flow, once the model run starts,".

Line 451. "Dissolution of En and Fo occurs in all the profile, while precipitation of Srp I and Srp II occurs in all the profile, except at the top" has been changed by "Dissolution of En and Fo occurs all along the profile, while precipitation of Srp I and Srp II occurs along the profile, except at the top."

Line 454. "As Srp I and Srp II react at equilibrium" What does react mean?

React means precipitate. The sentence has been removed as it was already said in the sentence before.

Line 457. "However, at the top of the profile, where rainwater is acidifying the system," has not been modified as proposed by Prof. G.Beaudoin.

Prof. G.Beaudoin is right in saying that rainwater is slightly acid, but we wanted to emphasize the effect of what this water does on the system.

Line 480. "On one hand, Fo_{90} is exhausted, which means that the only processes controlling Ni concentration in solution are the formation of Srp I or Srp II and the sorption of Ni onto goethite surface."

But Srp I formed by hydrothermal fluids before weathering.

Text has been changed to "On one hand, Fo_{90} is exhausted, which means that the only processes controlling Ni concentration in solution are the formation of Srp II and the sorption of Ni onto goethite surface."

Line 499. "From this moment, saprolite horizon develops faster". How?

Text has been changed to "From this moment, saprolite horizon develops faster given that no more Ni can sorb onto goethite and it is available for serpentine precipitation".

Line 515. ">Fe_ONi$^+$ is the main surface species (Fig. 6)" has been changed by "The main surface species is >Fe_ONi$^+$". Ionic, as Prof. Beaudoin suggested is not added, as surface species can also be neutral.

Line 521. "one considered in the model, where despite assuming saturated conditions, O_2(g) and CO_2(g) are available throughout the column". What do you mean?

As explained previously in "Reference case section", and in order to simulate the effect of unsaturated flow, once the model run starts, porewater is equilibrated with atmospheric O_2(g) and CO_2(g) all along the profile.

The text has been changed to "The larger thickness of the limonitic horizon in relation to that of saprolite has been observed in areas with maximum lixiviation (Butt and Cluzel 2013) and unsaturated conditions, i.e. porewater in equilibrium with atmospheric O_2(g) and CO_2(g)".

Line 567. "To account for the variability of compositions observed in the field" of what?

Of serpentine II, it has been modified. "To account for the variability of compositions of Srp II observed in the field, two more chemical compositions have been used in the sensitivity analyses ***Srp II**** and ***Srp II***$^{\$}$ (Table 4)."

*Line 605. "*All Mg and nearly 40% of Ni have been leached from the system, while leaching of Si is reduced to 15% (Fig. 7)".Would imply Mg and Ni go out from the system?

Yes. Leaching of Mg, Si and Ni from laterites profiles developed over peridotites has been observed. (Butt and Cluzel 2013, Ulrich et al. 2014, Villanova-de-Benavent et al. 2016a).

Line 612. "These small saturation indices might not be enough to allow the precipitation of quartz" has been changed by "These small saturation indices might not be enough to overcome a kinetic barrier for the precipitation of quartz".

Line 614. "kinetically limited precipitation" Meaning?

It means a kinetically controlled precipitation. Text has been changed by "kinetically controlled precipitation of quartz".

Line 620. "Numerical model considers a 1D column of 88 m length initially composed of Fo90, En90, Srp I and Mag". The correction proposed by Prof. G.Beaudoin "Numerical models considering a 1D column of 88 m length initially composed of Fo90, En90, Srp I and Mag" has not been accepted as the sentence loses its sense.

Line 905. "Fig. 4 Evolution of the amount of mineral (in wt.%) (areas) and of the amount of Ni sorbed onto goethite (in wt.% of Ni in goethite) (solid line) and porosity in the profile at initial time (0 y) and at different model elapsed times (from 10^3 to 10^6 years) for the Reference case".

We do not change this sentence as we effectively refer to the amount of mineral in wt%.

Line 908 "Fig. 5. Evolution of pH in the profile at different model elapsed times for the Reference case." has been changed by "Fig. 5. pH distribution at the profile at different time steps for the Reference case".

Page 73. Table 1 has been moved to online resources and is referred as Online resource 1. The text has been modified accordingly.

Table 1

	Boundary porewater		**Initial porewater**	
	Concentration (mol/L)	Constraint	Concentration (mol/L)	Constraint
pH	4.5	Fixed	9.5	Equilibrium with Mag and Srp I
$O_2(g)$		Equilibrium $O_2(g)$ (0.21 atm)		Equilibrium with Mag
Eh (V)	0.9		-0.4	
CO_3^{2-}	1.4×10^{-5}	Equilibrium with $CO_2(g)$ ($10^{-3.4}$ atm)	1.0×10^{-8}	Fixed
Cl	4.3×10^{-5}	Fixed	1.0×10^{-4}	Fixed
Fe	1.0×10^{-10}	Fixed	2.1×10^{-8}	Equilibrium with Mag
Si	1.0×10^{-10}	Fixed	3.1×10^{-5}	Equilibrium with Srp I
K	5.0×10^{-6}	Fixed	1.0×10^{-9}	Fixed
Mg	5.0×10^{-7}	Fixed	1.5×10^{-5}	Equilibrium with Srp I
Na	1.0×10^{-4}	Charge balanced	1.0×10^{-4}	Charge balanced
Ni	1.0×10^{-15}	Fixed	4.6×10^{-8}	Equilibrium with Srp I

Table 1

Table 2

Mineral	Formula	% volume
Srp I	$Mg_{2.85}Fe_{0.14}Ni_{0.01}Si_2O_5(OH)_4$	50
En_{90}	$Mg_9FeSi_{10}O_{30}$	27
Fo_{90}	$Mg_9Fe_{0.95}Ni_{0.05}Si_5O_{20}$	6
Mag	$Fe_{2.97}Ni_{0.03}O_4$	5

Table 2

Table 3

mineral	reaction	log K	reference
Fa	$Fe_2SiO_4 + 4H^+ = 2Fe^{2+} + H_4SiO_4$	19.11	Wolery (1992)
Fo	$Mg_2SiO_4 + 4H^+ = 2Mg^{2+} + H_4SiO_4$	27.86	
En	$MgSiO_3 + 2H^+ + H_2O = Mg^{2+} + H_4SiO_4$	11.33	
Fs	$FeSiO_3 + 2H^+ + H_2O = Fe^{2+} + H_4SiO_4$	7.45	
Ni_2SiO_4	$Ni_2SiO_4 + 4H^+ = 2Ni^{2+} + H_4SiO_4$	19.43	This study, from data of Gamsjager et al. (2005)
Lz	$Mg_3Si_2O_5(OH)_4 + 6\ H^+ = 3\ Mg^{2+} + 2H_4SiO_4 + H_2O$	33.100 ± 0.900	Giffaut et al. (2014)
Gre	$Fe_3Si_2O_5(OH)_4 + 6\ H^+ = 3\ Fe^{2+} + 2H_4SiO_4 + H_2O$	21.77	
Nep	$Ni_3Si_2O_5(OH)_4 + 6\ H^+ = 3\ Ni^{2+} + 2\ H_4SiO_4 + H_2O$	19 ± 4	Villanova-de-Benavent et al. (2016a)
Fe(III)-Lz	$Fe_2Si_2O_5(OH)_4 + 6\ H^+ = 2\ Fe^{3+} + 2\ H_4SiO_4 + H_2O$	-1 ± 4	

Table 3

Table 4

Mineral	Reaction	Log K
Fo90	$Mg_9Fe_{0.95}Ni_{0.05}Si_5O_{20} + 20\ H^+ = 9\ Mg^{2+} + 0.95\ Fe^{2+} + 0.05\ Ni^{2+} + 5\ H_4SiO_4$	134.8
En90	$Mg_9FeSi_{10}O_{30} + 20\ H^+ + 10\ H_2O = 9\ Mg^{2+} + Fe^{2+} + 10\ H_4SiO_4$	109.3
Srp I	$Mg_{2.85}Fe_{0.14}Ni_{0.01}Si_2O_5(OH)_4 + 6\ H^+ = 2.85\ Mg^{2+} + 0.14\ Fe^{2+} + 0.01\ Ni^{2+} + 2\ H_4SiO_4 + H_2O$	32.5
Srp II	$Mg_{2.798}Fe_{0.102}Ni_{0.049}Si_2O_5(OH)_4 + 6\ H^+ = 2.798\ Mg^{2+} + 0.102\ Fe^{3+} + 0.049\ Ni^{2+} + 2\ H_4SiO_4 + H_2O$	31.0
Srp II*	$Mg_{2.789}Fe_{0.114}Ni_{0.040}Si_2O_5(OH)_4 + 6\ H^+ = 2.789\ Mg^{2+} + 0.114\ Fe^{3+} + 0.040\ Ni^{2+} + 2\ H_4SiO_4 + H_2O$	30.8
Srp II$	$Mg_{2.821}Fe_{0.084}Ni_{0.053}Si_2O_5(OH)_4 + 6\ H^+ = 2.821\ Mg^{2+} + 0.084\ Fe^{3+} + 0.053\ Ni^{2+} + 2\ H_4SiO_4 + H_2O$	31.3

Table 4

Table 5

	log K (2.31 sites/nm^2)	**reference**	**log K_o** (6.5 sites/nm^2)
>Fe_OH + H^+ = >Fe_OH_2^+	7.0	Richter and Brendler (2008)	6.6
>Fe_OH = >Fe_O^- + H^+	-9.4	Richter and Brendler (2008)	-9.8
>Fe_OH + Ni^{2+} = >Fe_ONi^+ + H^+	-0.4	Marcusen et al.(2009)	-0.8

Table 5

Table 6

	Reference case	Sensitivity analyses					
		No_ads	**Srp II***	**Srp II$**	**Rate**	**Less-carb**	**Qt**
Sorption Ni	Yes	No	Yes	Yes	Yes	Yes	Yes
Srp II composition	Srp II	Srp II	Srp II*	Srp II$	Srp II	Srp II	Srp II
Reactive area En_{90}/Fo_{90} (m^2/g)	$5\times10^{-3}/5\times10^{-4}$	$5\times10^{-3}/5\times10^{-4}$	$5\times10^{-3}/5\times10^{-4}$	$5\times10^{-3}/5\times10^{-4}$	$10^{-1}/10^{-1}$	$5\times10^{-3}/5\times10^{-4}$	$5\times10^{-3}/5\times10^{-4}$
Equil. with atm O_2 (g) and CO_2(g)	All nodes	All nodes	All nodes	All nodes	All nodes	Only rainwater	All nodes
Precipitation of Qt	No	No	No	No	No	No	Yes

Table 6

Figure1

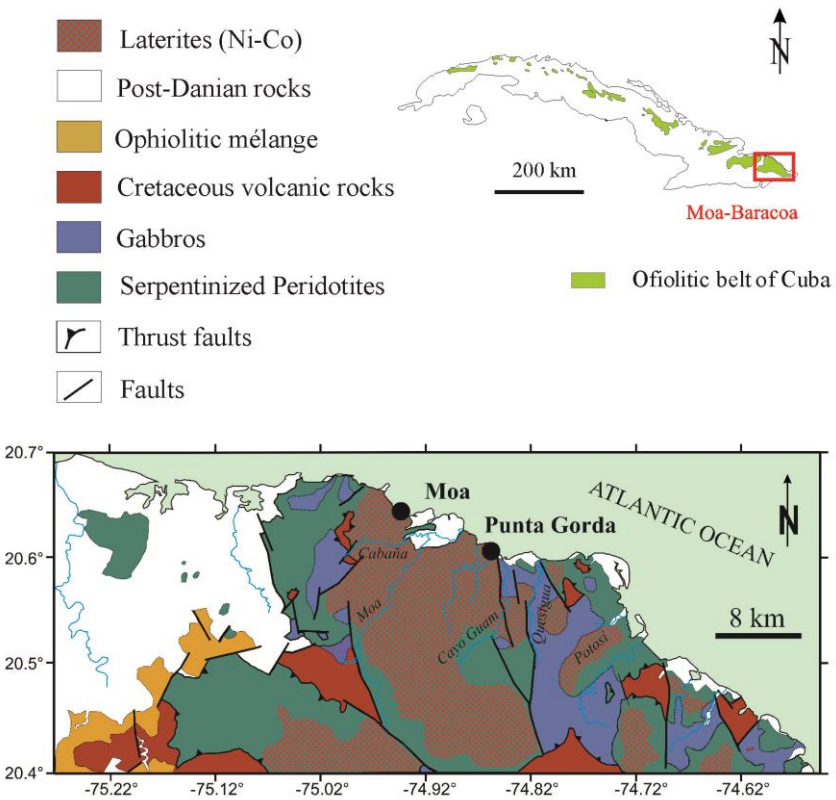

Figure 1

Figure 1 in jpg

Click here to download Figure Figure_1 Cristina D.jpg

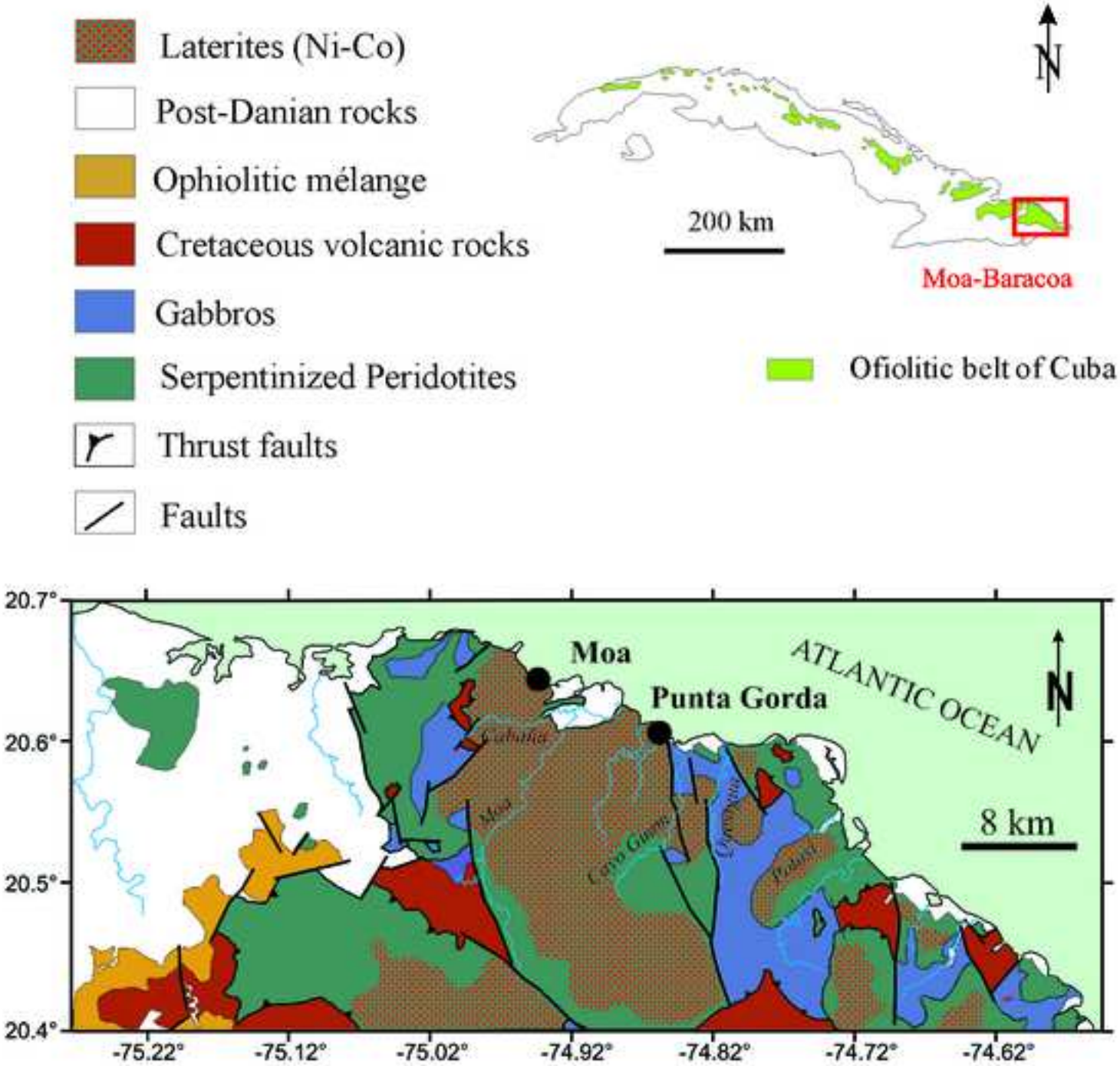

Figure 2

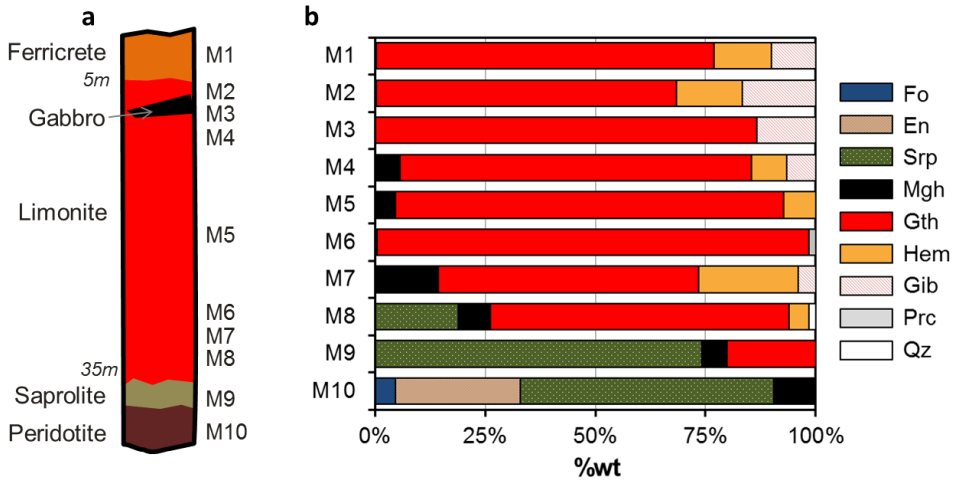

Figure 2

Figure 3

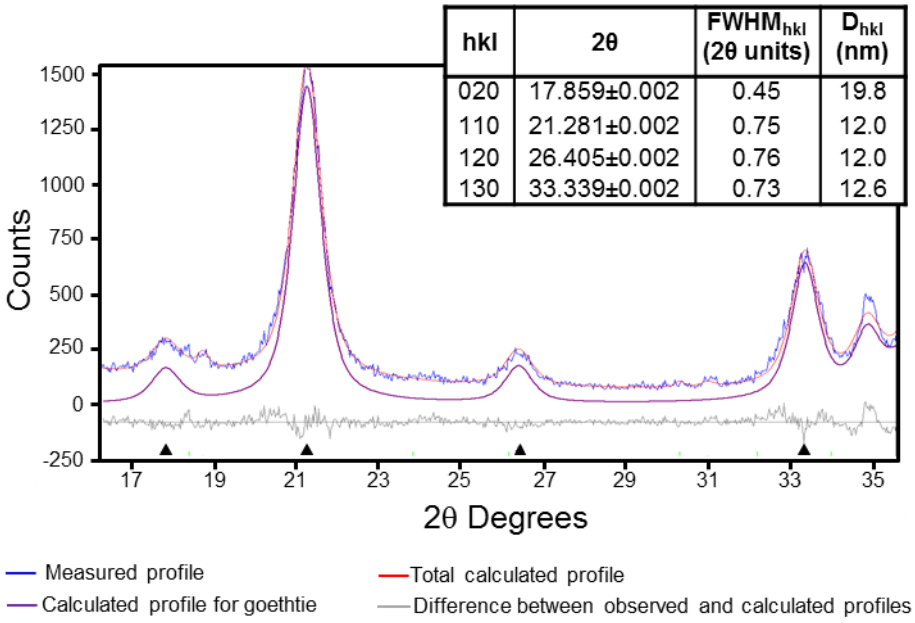

hkl	2θ	$FWHM_{hkl}$ (2θ units)	D_{hkl} (nm)
020	17.859±0.002	0.45	19.8
110	21.281±0.002	0.75	12.0
120	26.405±0.002	0.76	12.0
130	33.339±0.002	0.73	12.6

Figure 3

Figure 4

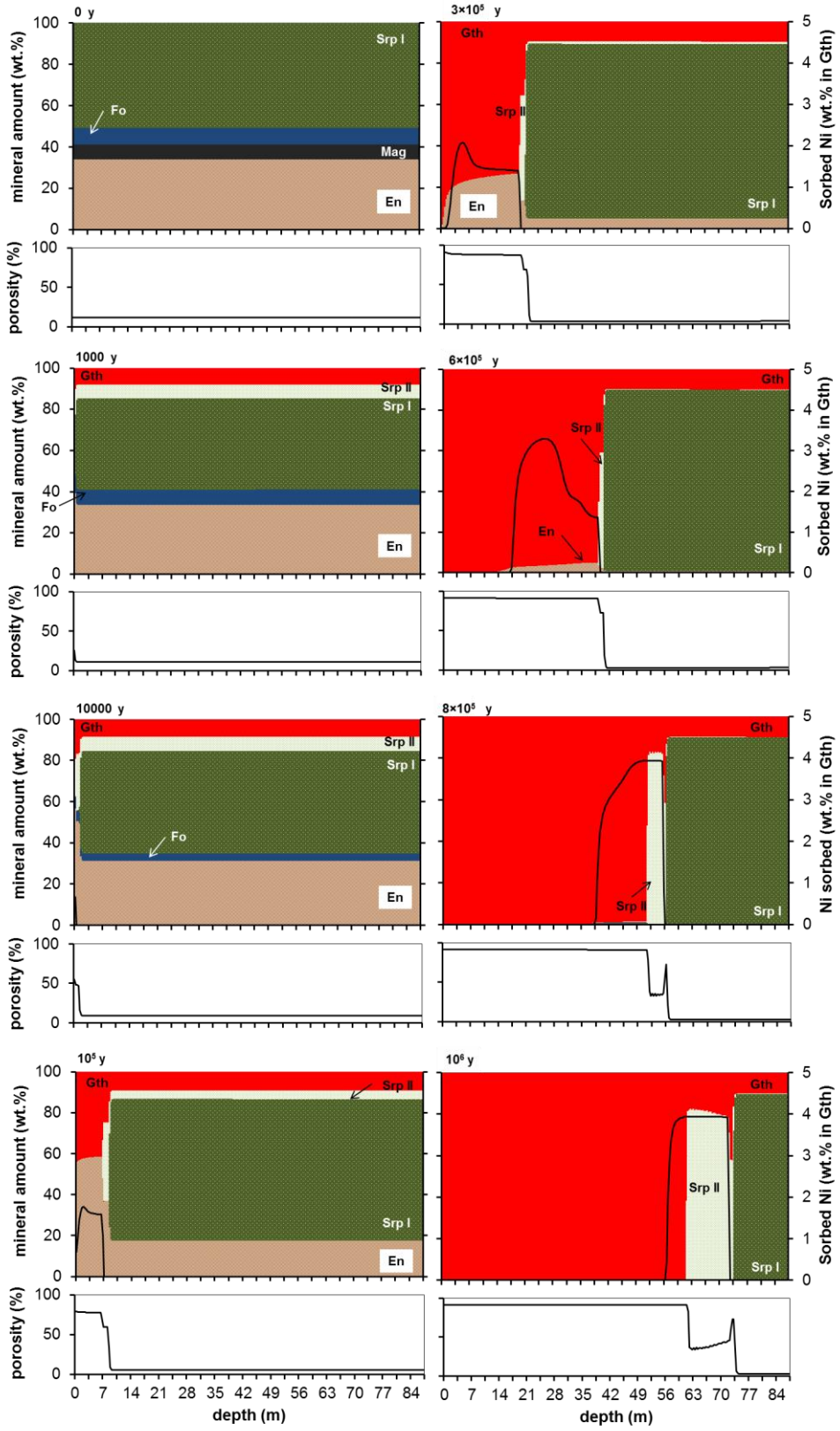

Figure 4

Figure 5

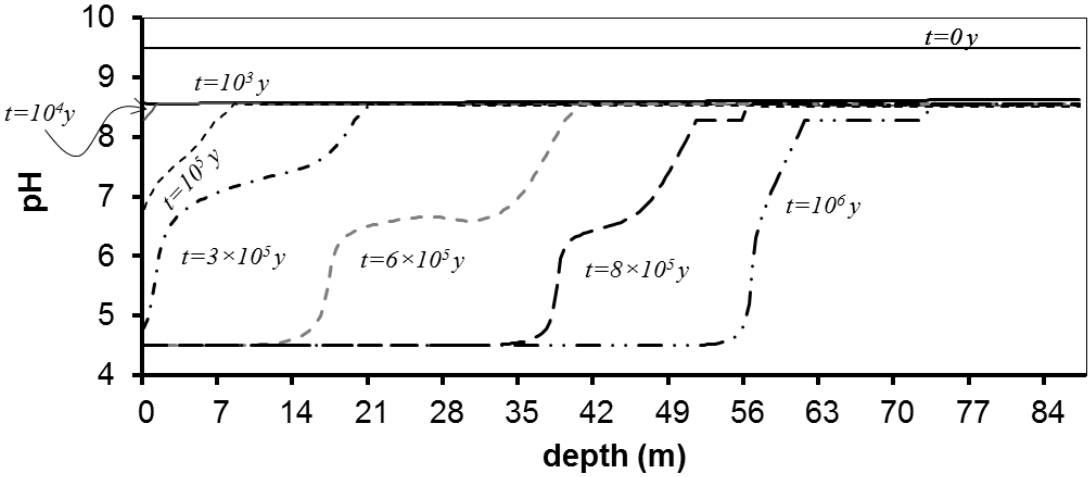

Figure 5

Figure 6

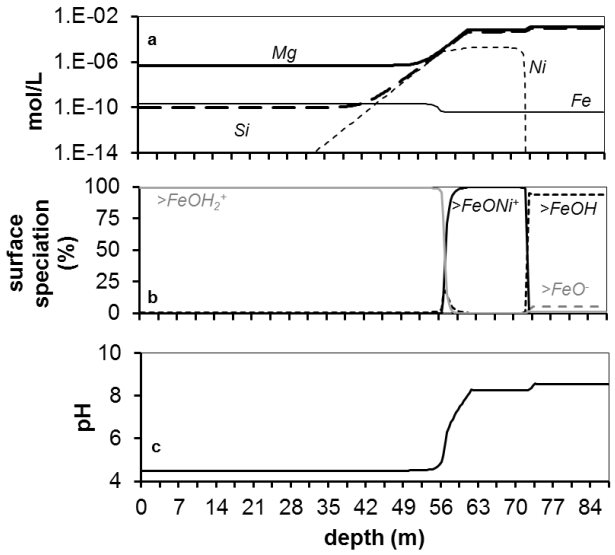

Figure 6

Figure 7

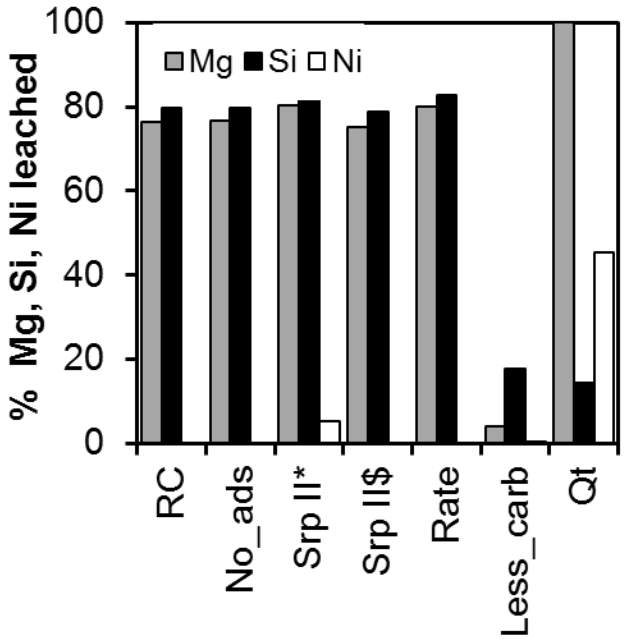

Figure 7

Figure 8

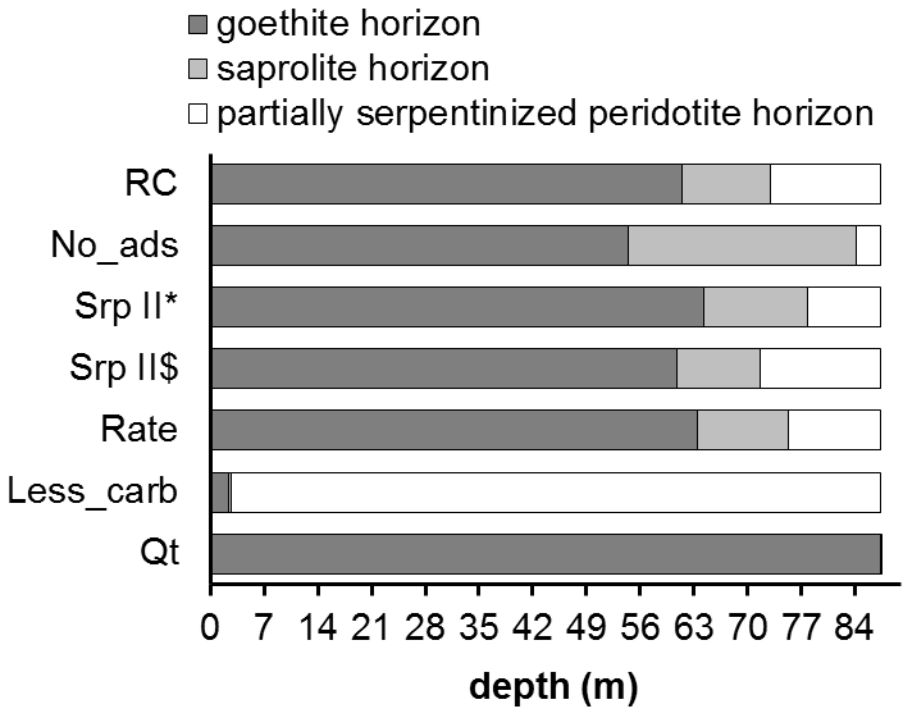

Figure 8

Figure 9

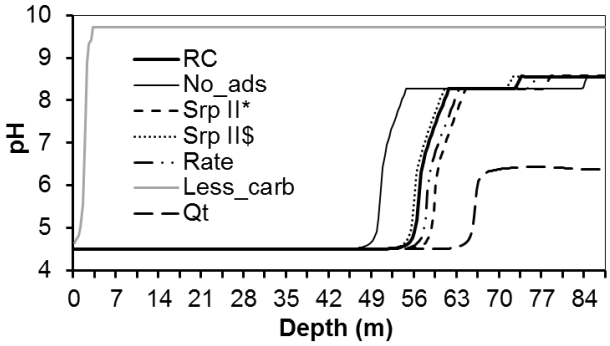

Figure 9

Click here to access/download
Supplementary Material
onlineresources.pdf